

# **The Great Deceiver: miR-2392's Hidden Role in Driving SARS-CoV-2 Infection**

J. Tyson McDonald<sup>1,2</sup>, Francisco Javier Enguita<sup>1,3</sup>, Deanne Taylor<sup>1,4,5</sup>, Robert J. Griffin<sup>1,6</sup>, Waldemar Priebe<sup>1,7</sup>, Mark R. Emmett<sup>1,8</sup>, Marisa McGrath<sup>9</sup>, Mohammad M. Sajadi<sup>9</sup>, Anthony D. Harris<sup>10</sup>, Jean Clement<sup>9</sup>, Joseph M. Dybas<sup>1,4</sup>, Nukhet Aykin-Burns<sup>11</sup>, Joseph W. Guarnieri<sup>1,12</sup>, Larry N. Singh<sup>1,12</sup>, Peter Grabham<sup>1,13</sup>, Stephen B. Baylin<sup>1,14</sup>, Aliza Yousey<sup>1,15</sup>, Andrea N. Pearson<sup>15</sup>, Peter M. Corry<sup>1,6</sup>, Amanda Saravia-Butler<sup>1,16,17</sup>, Thomas R. Aunins<sup>18</sup>, Prashant Nagpal<sup>19,20,21</sup>, Cem Meydan<sup>22,23</sup>, Jonathan Foox<sup>22,23</sup>, Christopher Mozsary<sup>22,23</sup>, Bianca Cerqueira<sup>1,24,25</sup>, Viktorija Zaksas<sup>1,26</sup>, Urminder Singh<sup>1,27</sup>, Eve Syrkin Wurtele<sup>1,27</sup>, Sylvain V. Costes<sup>17</sup>, Diego Galeano<sup>1,28,29</sup>, Alberto Paccanaro<sup>1,28,30</sup>, Suzanne L. Meinig<sup>31</sup>, Robert S. Hagan<sup>31,32</sup>, Natalie M Bowman<sup>33</sup>, UNC COVID-19 Pathobiology Consortium<sup>34,35+</sup>, Matthew C. Wolfgang<sup>31,35</sup>, Selin Altinok<sup>36</sup>, Nicolae Sapoval<sup>1,37</sup>, Todd J. Treangen<sup>1,37</sup>, Matthew Frieman<sup>1,9</sup>, Charles Vanderburg<sup>38</sup>, Douglas C. Wallace<sup>1,12</sup>, Jonathan Schisler<sup>1,36</sup>, Christopher E. Mason<sup>1,22,23,39,40</sup>, Anushree Chatterjee<sup>1,18,19,20</sup>, Robert Meller<sup>1,15</sup>, Afshin Beheshti<sup>1,38,41,42,43\*</sup>

<sup>1</sup>COVID-19 International Research Team

<sup>2</sup>Department of Radiation Medicine, Georgetown University School of Medicine, Washington D.C. 20007, USA

<sup>3</sup>Instituto de Medicina Molecular João Lobo Antunes, Faculdade de Medicina, Universidade de Lisboa, Av. Prof. Egas Moniz, 1649-028 Lisbon, Portugal

<sup>4</sup>Department of Biomedical and Health Informatics, The Children's Hospital of Philadelphia, Philadelphia, PA 19104 USA

<sup>5</sup>Department of Pediatrics, Perelman School of Medicine, University of Pennsylvania, Philadelphia, PA 19104 USA

<sup>6</sup>Radiation Biology Division, Dept of Radiation Oncology, University of Arkansas for Medical Sciences, Little Rock, AK, 72211 USA

<sup>7</sup>Department of Experimental Therapeutics, University of Texas MD Anderson Cancer Center, Houston, TX, 77030, USA

<sup>8</sup>Department of Biochemistry and Molecular Biology, University of Texas Medical Branch, Galveston, TX 77555, USA

<sup>9</sup>Institute of Human Virology, University of Maryland School of Medicine, Baltimore, MD, 21201, USA

<sup>10</sup>Department of Epidemiology and Public Health, University of Maryland School of Medicine, Baltimore, MD, 21201, USA

<sup>11</sup>Division of Radiation Health, Department of Pharmaceutical Sciences, University of Arkansas for Medical Sciences, Little Rock, AK, 72211 USA

<sup>12</sup>Center for Mitochondrial and Epigenomic Medicine, Children's Hospital of Philadelphia, Philadelphia, PA 19104, USA

<sup>13</sup>Center for Radiological Research, Columbia University, New York, NY 10032, USA

<sup>14</sup>Department of Oncology, Sidney Kimmel Comprehensive Cancer Center, Johns Hopkins School of Medicine, Baltimore, MD 21287, USA

<sup>15</sup>Department of Neurobiology and Pharmacology, Morehouse School of Medicine, Atlanta, GA 30310, USA

<sup>16</sup>Logyx, LLC, Mountain View, CA 94043, USA

- <sup>17</sup>Space Biosciences Division, NASA Ames Research Center, Moffett Field, CA 94035, USA
- <sup>18</sup>Department of Chemical and Biological Engineering, University of Colorado Boulder, Boulder, CO, 80303, USA
- <sup>19</sup>Sachi Bioworks Inc, Boulder, CO, 80301, USA
- <sup>20</sup>Antimicrobial Regeneration Consortium, Boulder, CO, 80301, USA
- <sup>21</sup>Quantum Biology Inc, Boulder, CO, 80301, USA
- <sup>22</sup>Department of Physiology, Biophysics and Systems Biology, Weill Cornell Medicine, NY, 10065, USA
- <sup>23</sup>The HRH Prince Alwaleed Bin Talal Bin Abdulaziz Alsaud Institute for Computational Biomedicine, Weill Cornell Medicine, NY, 10065, USA
- <sup>24</sup>KBR Space & Science, San Antonio, TX, 78235, USA
- <sup>25</sup>Aeromedical Neurology & Neuroimaging Research Group, United States Air Force School of Aerospace Medicine, Lackland AFB, TX, 78236, USA
- <sup>26</sup>Center for Translational Data Science, University of Chicago, Chicago, IL, 60615, USA
- <sup>27</sup>Bioinformatics and Computational Biology Program, Center for Metabolic Biology, Department of Genetics, Development and Cell Biology, Iowa State University, Ames, IA 50011, USA
- <sup>28</sup>School of Applied Mathematics, Fundação Getulio Vargas, Rio de Janeiro, Brazil
- <sup>29</sup>Faculty of Engineering, National University of Asuncion, Central, Paraguay
- <sup>30</sup>Department of Computer Science, Centre for Systems and Synthetic Biology, Royal Holloway, University of London, Egham Hill, Egham, UK
- <sup>31</sup>Marsico Lung Institute, University of North Carolina at Chapel Hill, Chapel Hill, NC, 27599, USA
- <sup>32</sup>Division of Pulmonary Diseases and Critical Care Medicine, Department of Medicine, University of North Carolina, Chapel Hill, NC 27599, USA
- <sup>33</sup>Division of Infectious Disease, School of Medicine, University of North Carolina, Chapel Hill, NC, 27599, USA
- <sup>34</sup>Department of Oral and Craniofacial Health Sciences, UNC Adams School of Dentistry, University of North Carolina School of Medicine, Chapel Hill, NC, 27599, USA
- <sup>35</sup>Department of Microbiology & Immunology, University of North Carolina School of Medicine, Chapel Hill, NC, 27599, USA
- <sup>36</sup>McAllister Heart Institute, Department of Pharmacology, and Department of Pathology and Lab Medicine, The University of North Carolina at Chapel Hill, NC 27599, USA
- <sup>37</sup>Department of Computer Science, Rice University, Houston, TX 77005, USA
- <sup>38</sup>Stanley Center for Psychiatric Research, Broad Institute of MIT and Harvard, Cambridge, MA, 02142, USA
- <sup>39</sup>New York Genome Center, NY, USA
- <sup>40</sup>The Feil Family Brain and Mind Research Institute, Weill Cornell Medicine, NY, 10065, USA
- <sup>41</sup>KBR, Space Biosciences Division, NASA Ames Research Center, Moffett Field, CA, 94035, USA
- <sup>42</sup>Senior author
- <sup>43</sup>Lead Contact
- +The full list of authors associated with the UNC COVID-19 Pathobiology Consortium is available in the supplemental information.

\*Correspondence: [afshin.beheshti@nasa.gov](mailto:afshin.beheshti@nasa.gov)

## Summary (150 words)

MicroRNAs (miRNAs) are small non-coding RNAs involved in post-transcriptional gene regulation that have a major impact on many diseases and provides an exciting avenue towards antiviral therapeutics. From patient transcriptomic data, we have discovered a circulating miRNA, miR-2392, that is directly involved with SARS-CoV-2 machinery during host infection. Specifically, we found that miR-2392 was key in driving downstream suppression of mitochondrial gene expression, increasing inflammation, glycolysis, and hypoxia as well as promoting many symptoms associated with COVID-19 infection. We demonstrate miR-2392 is present in the blood and urine of COVID-19 patients tested, but not detected in COVID-19 negative patients. These findings indicate the potential for developing a novel, minimally invasive, COVID-19 detection method. Lastly, using both *in vitro* human and *in vivo* hamster models, we have developed a novel miRNA-based antiviral therapeutic targeting miR-2392 that significantly reduces SARS-CoV-2 viability and may potentially inhibit a COVID-19 disease state in the host.

## Key words

COVID-19, SARS-CoV-2, microRNA, miRNA, Facile Accelerated Specific Therapeutic (FAST), FASTmer, miR-2392, antiviral therapeutic

## Introduction

In Fall of 2019, the zoonotic spillover event led to the first know human infection with the severe acute respiratory syndrome coronavirus 2 (SARS-CoV-2) and subsequent human-to-human transmission triggered a pandemic leading to a worldwide health crisis from the resulting disease, referred to as coronavirus disease 2019 (COVID-19) (Huang et al., 2020; Zhu et al., 2020). COVID-19 causes substantial pulmonary disease but can also cause systemic health risks from extrapulmonary manifestations. Its effects entangle the entire body including but not limited to the cardiovascular, gastrointestinal, and hematological systems that may lead to long lasting effects after the virus has left the body, known as PASC (post-acute sequela of COVID-19) (Carfi et al., 2020; Feng et al., 2020; Gupta et al., 2020; Jacobs et al., 2020). SARS-CoV-2 is classified as a member of the Coronaviridae family, a group of viruses with a enveloped positive-stranded RNA that has the ability to infect cross-species (V'Kovski et al., 2021). Currently, three novel vaccines have completed efficacy trials and have been approved for emergency use by the Food and Drug Administration (Baden et al., 2021; Polack et al., 2020; Sadoff et al., 2021). While these vaccines represent a favorable milestone, additional data is required to demonstrate the long-term effectiveness against SARS-CoV-2 and protection against new strains. To prevent an endemic, the complete global eradication of COVID-19 will require a wide majority of the world's population to be vaccinated to achieve herd immunity. Unfortunately, there will always be a portion of the population that will not get vaccinated. Therefore, additional strategies for antiviral therapeutic options against COVID-19 are particularly relevant and important to explore in order to treat severe illnesses and overcome this global pandemic. Currently the majority of antivirals are repurposed drugs utilized for other disease and have shown limited clinical

efficacy, such as remdesivir (Abdelrahman et al., 2021). This brings a needed urgency to develop antivirals specifically designed against SARS-CoV-2.

One potential avenue for an alternative antiviral agent is treatment against specific microRNAs (miRNAs) associated with SARS-CoV-2 infection and subsequent manifestation of COVID-19. MicroRNAs (miRNAs) are non-coding RNAs that are involved with regulation of post-transcriptional gene expression and can impact entire pathways related to viruses and diseases (Jiang et al., 2009; Trobaugh and Klimstra, 2017). Each miRNA can target multiple messenger RNAs (mRNAs) and taken together, miRNAs are predicted to regulate over half of the human transcriptome (Friedman et al., 2009). Recent evidence has shown different diseases, including COVID-19, leads to distinct complements of miRNAs in the blood (Mishra et al., 2020; Nersisyan et al., 2020; Portincasa et al., 2020; Sacar Demirci and Adan, 2020; Sardar et al., 2020; Teodori et al., 2020; Widiasta et al., 2020; Zhang et al., 2021). These circulating miRNAs are highly stable and have the potential to be used for minimally invasive novel detection, potential biomarkers, and therapeutic targets (Tribolet et al., 2020). Research on the interactions between miRNAs and viruses have revealed a multifaceted relationship. Specifically, viruses have been shown to avoid the immune response by leveraging cellular miRNAs to complete their replication cycle (Trobaugh and Klimstra, 2017). The following mechanisms are central to the interaction of viruses and miRNAs: 1) miRNA processing pathways can be blocked or inhibited by viruses interacting with key proteins such as Dicer and associated proteins, 2) viruses can sequester miRNAs resulting in dysregulation of specific target mRNAs, 3) viruses can utilize miRNAs to redirect regulatory pathways of other miRNA targets to provide survival advantages, and 4) viruses can directly encode miRNA precursors that are processed by the canonical miRNA cellular pathway and have well-defined functions to specifically target and regulate the viral replicative cycle (Schult et al., 2018; Trobaugh and Klimstra, 2017).

Here, we report on a miRNA, miR-2392, that may directly regulate and drive a COVID-19 response. This miRNA was initially predicted from COVID-19 patient data that consisted of multiple miRNAs being suppressed/inhibited (miR-10, miR-10a-5p, miR-1-3p, miR-34a-5, miR-30c-5p, miR-29b-3p, miR-155-5p, and miR-124-3p) and one miRNA being upregulated (miR-2392). With further examination, we discovered miR-2392 to be a key miRNA involved with COVID-19 progression. Specifically, miR-2392 drives downstream suppression of mitochondria activity while increasing inflammation, glycolysis, and hypoxia. MiR-2392 upregulation was concomitant with symptoms associated with COVID-19 infection in the host. We found that miR-2392 was circulating in COVID-19 infected patients and increased as a function of viral load. Our results demonstrate that miR-2392 may be utilized as an effective biomarker of COVID-19. Furthermore, we have developed a miR-2392 inhibitor and provide evidence that its use reduces SARS-COV-2 viability in targeted viral screens with A549 cells and reduces the impact of infection in COVID-19 animal models. With further development this miR-2392 inhibitor may represent an effective antiviral therapeutic towards inhibiting the virus and limiting a negative host response from COVID-19.

## Results



# *Identification of key miRNAs associated with COVID-19 infection*

Currently, the majority of the published literature associated with miRNAs and SARS-CoV-2 is based on *in silico* predictions. To identify miRNAs that may be involved in driving COVID-19 severity in the host, we first examined publicly available Bronchial Alveolar Lavage Fluid (BALF) RNA-sequencing (RNA-seq) data from 13 individuals. Differential gene expression was assessed using a 1.2-fold change in gene expression for p-values less than 0.01 revealing 42 increased genes and 347 decreased genes, compared to controls. Using the upstream regulator analysis from the Ingenuity Pathway Analysis (IPA) knowledge database, the miRNAs from differentially expressed genes (FDR < 0.05) from COVID-19-positive patients were inferred. Eight miRNAs were predicted to drive significant changes in COVID-19 positive patients with the downregulation of seven miRNAs (miR-10, miR-1, miR-34a-5p, miR-30c-5p, miR-29b-3p, miR-124-3p, and miR-155-5p) and upregulation of a single miRNA, miR-2392 (**Fig. 1A**). Using IPA's downstream effects analysis to predict biological processes from the combined suppression of the seven miRNAs and the upregulation of miR-2392 resulted in increased inflammation, immune suppression, and suppression of mitochondrial activity in the BALF dataset (**Fig. 1B and 1C**).

In support of these findings, previous studies have shown alterations in specific miRNAs may directly impact viral infections. For example, upregulation of miR-10, miR-124, or miR-1 have been shown to have antiviral roles during infection (Hu et al., 2020; Sardar et al., 2020; Yang et al., 2016). Interestingly, upregulation of miR-30 and miR-155 have been shown independently to provide suppression in other types of coronaviruses (Dickey et al., 2016; Ma et al., 2018). The one miRNA predicted to be upregulated in COVID-19 patients from the BALF data was miR-2392. Though limited, the existing literature on miR-2392 demonstrates it is related to mitochondrial suppression and increased glycolysis (Fan et al., 2019) and circulating factors related to negative health risks (Chen et al., 2013; Fan et al., 2019; Hou et al., 2019; Li et al., 2017; Park et al., 2014; Yang et al., 2019).

Pathway analysis was performed with targets and pathways for miR-2392 to determine its impact on the host when upregulated. We observed that the upregulation of miR-2392 in the RNA-seq dataset impacted many downstream targets and pathways related to negative health outcomes (**Fig. 1C**). In addition to mitochondrial suppression, we also predicted activation of factors related to reactive oxygen species (ROS). Alternatively, since it is known that miR-2392 directly interacts with the mitochondrial DNA (mtDNA) to inhibit the levels of many of the mtDNA coded oxidative phosphorylation transcripts, this could be a compensatory response to the inhibition of mitochondrial bioenergetics.

Glycolytic pathways (**Fig. 1C**) are also upregulated in association with increased miR-2392. MiR-2392 drives both hexokinase 2 (HK2) and pyruvate kinase (PKM) which are both positive regulators of glycolysis. HK2 phosphorylates glucose to produce glucose-6-phosphate and is a primary regulator of glycolysis. HK2 further enhances GDP-glucose biosynthesis. GDP-glucose is a nucleotide sugar which an essential substrate for all glycosylation reactions (i.e. glycosylation of viral spike proteins). Pyruvate kinase is essential for the production of ATP in glycolysis as this enzyme catalyzes the transfer of the phosphate group from phosphoenolpyruvate to ADP to make ATP. The mechanism of how miR-2392 is driving these

pathways is not clearly understood, but one possibility could be due to the stabilization of glycolytic transcripts.

Overall, the miR-2392 observed upregulation of glycolysis and antiviral effects related to miR-2392 suppression are consistent with the recently documented role of glucose metabolism in the progression of viral infection and poor outcome of COVID-19 (Ardestani and Azizi, 2021). It is also consistent with the reported effects of suppression of glycolysis by inhibitors like the glucose analog, 2-deoxy-D-glucose (2-DG), that was shown to suppress SARS-CoV-2 replication in *in vitro* models (Ardestani and Azizi, 2021; Bojkova et al., 2020; Codo et al., 2020). Interestingly, 2-DG is also 2-deoxy-D-mannose and as such can interfere with processes utilizing mannose, a monosaccharide that is *in vivo* produced from glucose. Mannose plays important roles in the glycosylation of specific proteins. Replacement of a mannose molecule by 2-DG in the respective SARS-CoV-2 N-glycans or O-glycans might lead to their truncation and subsequently to the suppression of virus infectivity and proliferation. These and miR-2392 data clearly indicate that selective targeting of glucose metabolism might have significant impact on current and future SARS-CoV-2 pandemics.

Targets related to the goals of antioxidant N-acetyl cysteine (NAC) therapy are also observed to be upregulated. These include activated endothelial cell increasing their expression of numerous adhesion molecules, including intercellular adhesion molecule 1 (ICAM1), vascular cell adhesion molecule 1 (VCAM1), and E-selectin, which allow attachment of hematopoietic immune and non-immune cells to the endothelial surface, and thus, contribute to inflammation and activation of the coagulation cascade. Powerful antioxidants such as NAC counteract COVID19 infections by potentially suppressing viral replication via improving intracellular thiol redox ratio as a precursor for major thiol antioxidant glutathione (Ho and Douglas, 1992) and inhibiting the NF- $\kappa$ B pathway (Poppe et al., 2017). Inhibition of the NF- $\kappa$ B pathway has been shown to reduce inflammatory damage by altering the glutathione and glutathione disulfide ratio (Aykin-Burns et al., 2005; Griffin et al., 2003; Jia et al., 2010). Because NAC can also modulate oxidative burst and reduce cytokine storm without weakening the phagocytizing function of neutrophils (Allegra et al., 2002; Kharazmi et al., 1988; Sadowska et al., 2006), its use in COVID-19 patients as a single agent or in combination with other antioxidants are being conducted in clinical trials (Alamdari et al., 2020). A recent study has shown noteworthy benefits of NAC in patients with severe COVID-19 infection (Ibrahim et al., 2020). Major mechanisms proposed for these favorable patient outcomes were NAC's ability to reduce IL-6 induced mitochondrial oxidative stress via Complex I inhibition as well as to prevent increased inflammation due to uncontrolled activation of mTORC1. These results were in line with the role of miR-2392 in reducing the activities of electron transport chain complexes and enhancing glycolysis, which is known to be induced by mTORC1 activation. The same study also speculated that NAC could inhibit SARS-CoV-2 binding to ACE2 by reducing disulfide bonds in its receptor-binding domain. Inflammatory pathways and others that are observed with COVID-19 infection were also seen to be activated downstream of miR-2392.

*Conservation of miR-2392 between species and its predicted interactions with the SARS-CoV-2 genome*

Viral miRNAs can play a role in interspecies transmission due to the high conservation of miRNAs among species and the ability of viruses to integrate miRNAs into its own genome (Sacar Demirci and Adan, 2020; Schult et al., 2018). In addition, such integration of miRNAs within the virus has been shown to assist viruses to replicate and evade the immune system (Islam and Islam, 2021). To determine if miR-2392 might be capable of driving the observed COVID-19 health risks and symptoms in the host, we analyzed the conservation of human miR-2392 across species and the integration of miR-2392 into the SARS-CoV-2 genome (**Fig. 2**).

The UCSC Genome Browser was utilized to determine the conservation of miR-2392 across different species (Kent et al., 2002). The mature 20 base-pair miR-2392 is derived from an 84 base-pair region of the 3'-UTR in the long non-coding RNA (lncRNA) gene, maternally expressed 3 (MEG3) and located in an imprinted region DLK1-DIO3 that also contains three clusters for the expression of 51 additional miRNAs (**Fig. 2A and 2B**). A base wise evolutionary conservation comparison demonstrated that miR-2392 is highly conserved among non-human primates. In addition, conservation of miR-2392 is evident in dogs, cats, and ferrets, species known to be infected with SARS-CoV-2 while mice and rats, species not impacted by COVID-19 (Johansen et al., 2020), have poor conservation with miR-2392.

To determine the impact of miR-2392 on normal tissues, we studied the impact of miR-2392's host gene, MEG3, on normal tissues utilizing GTEx data (Consortium, 2020). For the majority of healthy tissues, MEG3 was either not detected or being expressed at low levels (**Fig. 2B**). This can imply that miR-2392 does not seem to significantly affect normal tissues.

To explore potential binding sites for miR-2392, we used the miRanda software (Enright et al., 2003) to identify all potential binding sites with respect to the SARS-CoV-2 reference genome (Wuhan-Hu-1; NC045512.2) and representative genomes from lineages of concern. We found that the miR-2392 seeding region is heavily integrated within SARS-CoV-2 and conserved in different viral strains (**Fig. 2C**). The three best hits from the miRanda scores are located in the NSP2, NSP3, and E-genes. Notably, these regions were conserved among 6 variants and lineages of concern each represented by 14 recent genomes from the respective lineage available from the Global Initiative on Sharing All Influenza Data (GISAID, (Shu and McCauley, 2017)).

#### *MiR-2392 targets mitochondrial and inflammatory pathways associated with SARS-CoV-2*

To determine in more detail the specific impact of miR-2392 gene targets and pathways in COVID-19 patients, miR-2392 gene targets were retrieved from the miRmap database as predicted by base pairing with its seed-region (Vejnar and Zdobnov, 2012). This list was further refined by overlap found in several other miRNA databases including miRmap (Vejnar and Zdobnov, 2012), miRwalk (Dweep and Gretz, 2015), miRDB (Chen and Wang, 2020), miRnet (Chang et al., 2020b), and ClueGo (Bindea et al., 2009). We also included RNA-seq analysis of 39 autopsy tissue samples from the heart, lung, kidney, liver, and lymph node of COVID-19-positive patients with high or low viral loads (Park et al., 2021). The refined list of miR-2392 gene targets (consisting of 375 genes) was examined using volcano plots in all samples (**Fig. 3A-F**).

To better determine the systemic impact on miR-2392 gene targets in COVID-19, we performed pathway analysis from the nasopharyngeal swab samples in living donors with and without COVID-19 using the SARS-CoV-2 viral load as the independent variable (high,

medium, low, other virus). The miR-2392 gene targets are differentially expressed ( $FDR < 0.05$ ) in at least one comparison of COVID-19-positive patients or other detected virus and were found to separate into six distinct hierarchical clusters that were identified and annotated utilizing ShinyGO (Ge et al., 2020) to determine the major pathways altered (**Fig. 3G**). The majority of these upregulated miR-2392 targets are involved in immune and inflammatory pathways. The downregulated miR-2392 targets were involved in mitochondrial function, oxidative stress, cell cycle, developmental biology, and ubiquitin binding which are pathways recently associated with the SARS-CoV-2 infection process (Hemmat et al., 2021). This data demonstrates miR-2392 may target several gene pathways related to perpetuating SARS-CoV-2 infection. For the majority of the tissues (excluding the lymph nodes), higher viral loads are associated with greater miR-2392 gene targets being regulated. Interestingly, the lymph nodes show an inverse relationship with viral loads compared to other tissues.

Because miR-2392 was recently shown to directly target the transcription of mitochondrial DNA genes (Fan et al., 2019), we evaluated the impact on expression of the mitochondrial miR-2392 targets in our datasets. Differentially expressed miR-2392 target mitochondrial genes were identified using the MitoCarta database (Rath et al., 2021) (**Fig. 3H**). This revealed 14 genes harboring miR-2392 seed sequences that were significantly dysregulated in the nasal and heart samples. In nasal samples, SLC25A28, mitoferrin which mediates mitochondrial iron transport, was strongly upregulated along with IBA57, which is involved in iron sulfur assembly. The mitochondrial outer membrane protein import complex subunit TOMM20, cytochrome c oxidase (complex IV) subunit COX6B1, and mitochondrial transcription factor COT-2 (NR2F2) were strongly down regulated. In the heart, the folate enzyme MTHFD2L (methylenetetrahydrofolate dehydrogenase) was up-regulated while all of the other nuclear-coded mitochondrial genes identified were down regulated. Downregulated heart mitochondrial genes included NDUFS5 (complex I subunit), COX6B1 and COX10 (complex IV structural and assembly subunits), CKMT1A (mitochondrial creatine kinase), MRPL34 (subunit of the large subunit of the mitochondrial ribosome), COT-2 (NR2F2), AK4 and MSRB3 (adenylate kinase 4 and methionine-R-sulfoxide reductase which mitigate oxidative stress), MRS2 (magnesium transporter) and CLIC4 (chloride channel). The kidney showed mild upregulation of complex I and single methyl group metabolism, but down regulation of complex IV (COX10), regulatory factor (COT-2), and iron sulfur center protein (IBA57). Hence, SARS-CoV-2 seems to downregulate nuclear mitochondrial gene transcription in the more oxidative heart and kidney, as well as in nasal tissues.

Since inflammation is a key component of COVID-19 infection, we also overlaid the standard known inflammatory genes determined from Loza et al. (Loza et al., 2007) to the miR-2392 targets (**Fig. 3I**). The analysis reveals that, at the mRNA level, most of the complement pathway genes are upregulated in the tissue samples analyzed. These changes could be compensatory, as proteins encoded by the genes could be downregulated as a function of traditional miRNA effects. The responses reflect the importance of degrees of inflammation for mediation of disease severity in COVID-19 patients and a key modulatory role of miR-2392 in this context.

Proteomic and transcriptomic analysis on miR-2392 targets on blood from COVID patients utilizing COVIDome (Sullivan et al., 2021) revealed interesting patterns between RNA and



protein levels for miR-2392 targets (**Fig. 3J and 3K**). We utilized the miR-2392 gene targets only determined through miRmap to determine a broader relationship between the proteins and genes. Several miR-2392 targets in the tissue show a significant transcription increase in COVID-19-positive samples with small to no changes on the proteomics level: PLK1, CD38, PYCR1, RNASE1, BIRC5, RRM2, SIGLEC1 (**Fig. 3J**). Interestingly, all these genes were also positively regulated for the majority of tissues when considering only miR-2392 gene targets with miRmap (**Figs. S1 and S2**). In the blood, the miR-2392 targets CXCL10, STAT1, IFIT3, and C1QC were positively regulated at both the protein and gene levels. This upregulation was also observed in all other tissues (**Figs. S1 and S2**). We explored the correlation between RNA expression and protein abundance for miR-2392 targets in COVID-19 positive and negative samples (**Fig. 3K**). Pearson correlation in both sample types is very close, with a slightly stronger value in COVID-19 negative samples (negative samples  $\text{cor}=0.2089863$ ,  $\text{p-value}=4\text{e-}10$ , positive samples  $\text{cor}=0.2053345$ ,  $\text{p-value}=8\text{e-}10$ ). Further investigation is needed to understand if increased levels of miR-2392 could potentially bind genes' mRNAs at a higher rate and therefore prevent translation to protein or if there are other mechanisms preventing mRNA translation to protein.

#### *Overexpression of miR-2392 simulates a phenotype similar to COVID-19 infection*

To determine if the upregulation of miR-2392 alone would elicit effects similar to a COVID-19 infection, cells were treated with a miR-2392 mimic. Using RNA-seq data, there were 649 genes with a fold-change greater than  $\pm 1.2$  and a p-value less than 0.05 (**Fig. 4A**). A number of these differentially expressed genes were predicted targets of miR-2392 (**Fig. 4B**). Of particular interest are differentially expressed genes in this model that are also dysregulated in SARS-CoV-2 infected cells. We analyzed whole cell proteome data from a human-derived cell culture model for a SARS-CoV-2 infection profile (Stukalov et al., 2021), and found 10 proteins that were significantly changed in abundance and were also altered with miR-2392 overexpression: KIF22, FKBP14, RAD51, AFAP1, ZCCHC17, ZWINT, MAGED1, CENPF, TMEM70, and NFKB2 (**Fig. 4C**). Viral infection is associated with alterations in protein posttranslational modifications of cellular proteins, including ubiquitination. This phenomenon can occur by viral or host directed modifications. We analyzed the ubiquitinome of the human-derived cell culture model of SARS-CoV-2 infection and observed a number of proteins that were increased or decreased in normalized ubiquitin abundance and were also dysregulated genes by miR-2392 overexpression. Furthermore, we found miR-2392 overexpression impacted genes involved with mitochondria, and inflammation (**Fig. 4D-4F**).

To determine if there was a direct correlation between miR-2392 overexpression and SARS-CoV-2 infection, comparisons were made using gene expression fold-change values or overlap in statically significant curated gene sets from canonical pathways determined by our fGSEA analysis. Using previously published data from Blanco-Melo *et al.* (Blanco-Melo et al., 2020), showed there was a statistically significant and positive correlation of the miR-2392 treatment compared to both the A549 and Calu-3 cell culture models infected with SARS-CoV-2 (**Fig. 4G and 4H**) as well as in lung biopsies post-mortem from two COVID-19 positive patients (**Fig. 4H**). Using nasal swab samples, a significant and positive correlation was determined between patients with medium- and low-viral loads compared to non-infected patients (**Fig. 4I and 4J**).



Further identification of miR-2392 correlation to SARS-CoV-2 infections was made using RNA-seq from multiple tissues (heart, kidney, liver, lymph node, and lung) obtained during autopsies of COVID-19 patients with high or low viral loads (**Fig. 4I-J**). There was a positive correlation to lung and lymph node tissues with miR-2392 expression. Interestingly, there was a significant and positive correlation to liver tissue when comparing gene fold-change values (**Fig. 4I**) but not fGSEA curated biological genesets (**Fig. 4J**). In contrast, a negative correlation to heart tissue was observed.

Statistically significant pathways that were enriched due to miR-2392 treatment were examined using fGSEA (**Fig. 4K-O**). It was observed that the miR-2392 treatment induced pathway response that was significantly related to SARS-CoV-2 pathways. One obvious relationship shows that the Reactome SARS-CoV-2 pathways were significantly activated for the miR-2392 treated cells compared to the controls (**Fig. 4K and 4L**). Significant Hallmark pathways (**Fig. 4N**) show distinct pathways that have been reported to be associated with COVID-19 in patients, such as upregulation of hypoxia (Herrmann et al., 2020), glycolysis (Ardestani and Azizi, 2021), and cell cycle pathways (Su et al., 2020). Interestingly, the KEGG pathway analysis (**Fig. 4M**) indicates the overexpression of miR-2392 treated highly upregulated systemic lupus erythematosus which has been reported to occur in COVID-19 patients and have shown similar pathologies due to the increase of inflammation (Zamani et al., 2021).

Lastly, we determined the impact of miR-2392 specific targets being downregulated in the cell lines after miR-2392 overexpression. A regulatory network was built by including the predicted miR-2392 targets in the microRNA Data Integration Portal (MIRDIP) that were also downregulated in the overexpression cell model as well as from the recently described consensus transcriptional regulatory networks in coronavirus infected cells (Ochsner et al., 2020) (**Fig. 4P**). The gene enrichment analysis of these putative miR-2392 targets showed the presence of GO-terms related with the RNA metabolism, transcription, ribosome activity and Golgi complex (**Fig. 4Q**).

#### *Circulating miR-2392 and the suppression of other miRNAs in COVID-19 infected patients*

To demonstrate the presence of circulating miR-2392 in COVID-19 infected patients, we quantified the amount of miR-2392 by droplet digital PCR (ddPCR) in the serum, urine and nasopharyngeal swab samples (**Fig. 5**). For the serum there were ten COVID-19 positive intubated patients, ten COVID-19 positive patients (not intubated), and ten negative patients. For the urine samples there were 15 inpatient COVID-19 positive samples, 15 outpatient COVID-19 positive samples, 10 inpatient COVID-19 negative samples, and 11 COVID-19 negative healthy donors. Lastly, we quantified nasopharyngeal swab samples from 10 COVID-19 positive patient samples, 6 common cold coronavirus positive patient samples (229E, HKU1, and OC43), and 6 Respiratory Illness/Coronavirus NL63 positive patient samples. In addition, we also quantified three other miRNAs which we predicted to be inhibited by COVID-19 infection (**Fig. 1A**) which were: miR-1-3p (**Fig. S3**), miR-155-5p (**Fig. S4**), and miR-124-3p (**Fig. S5**).

We observed a statistically significant increase of miR-2392 in COVID-19 positive patients from both the serum and urine samples (**Fig. 5A**). In addition, Receiver Operating Characteristic (ROC) curve analysis revealed that miR-2392 is significantly associated with SARS-CoV-2 infection in patients (**Fig. 5B**) in all tissues. Lastly, when dissecting the amounts of miR-2392

with specific conditions associated with infection, we observe that more severely affected patients (i.e. intubated patients or patients in ICU), had higher presence of miR-2392 (**Fig. 5C**). Interestingly, low levels miR-2392 appeared in the nasopharyngeal location with no significant differences occurring between seasonal coronavirus samples. Since we hypothesize that miR-2392 is a primary initiator for systemic impact of the infection, this might indicate that miR-2392 does not strongly appear until the virus has established its presence in the body.

As mentioned above we also measured the quantity of miR-1-3p (**Fig. S3**), miR-155-5p (**Fig. S4**), and miR-124-3p (**Fig. S5**) and performed the same analysis. For miR-1-3p we observed significant suppression in the serum while no significant differences in the urine or nasopharyngeal samples (**Fig. S3**). MiR-1-3p is known to be beneficial for cardiovascular functions, with the inhibition of miR-1-3p leading to heart failure and heart disease (Condorelli et al., 2010). Similar response was observed for miR-155-5p with significant suppression in the serum while no significant differences in the urine or nasopharyngeal samples (**Fig. S4**). For miR-124-3p, we observed very low amounts (on average < 2 copies/5 ng RNA), for all conditions, which indicates that miR-124-3p is not circulating for any of the patients for any the conditions observed (**Fig. S5**). MiR-124-3p provides as an ideal miRNA negative control candidate for SARS-COV-2.

#### *Inhibiting miR-2392: a novel antiviral COVID-19 therapeutic*

The link that we found between miR-2392 and COVID-19 infection prompted us to ask whether we could develop effective antivirals for COVID-19 by inhibiting miR-2392. We used the Facile Accelerated Specific Therapeutic (FAST) platform to develop an effective antisense-based therapeutic against human miR-2392 (Aunins et al., 2020; Eller et al., 2021), termed SBCov207, for the treatment of COVID-19 (**Fig. 6A**). The FAST platform combines the four essential modules of drug development cycle (design, build, test, and learn) to optimize therapeutics against any gene and species of interest in less than a week. The anti-miR-2392 FASTmer was evaluated for efficacy and toxicity against a SARS-CoV-2 infection of the human lung cell line A549 (**Fig. 6B-D**). Treatment of uninfected A549 cells showed no cytotoxicity up to 20  $\mu$ M. The control nonsense FASTmer (SBCov208) showed no toxicity even up to 40  $\mu$ M. Treatment of A549 cells infected with SARS-CoV2 showed drastic improvement in cell viability with an average of 85% viral inhibition at 10  $\mu$ M (IC<sub>50</sub> of  $1.15 \pm 0.33$   $\mu$ M). In contrast, the control nonsense FASTmer showed significantly lower viral suppression (**Fig. 6E-G**). Human cell line-based infection models reaffirm that the anti-miR-2392 (SBCov207) is effective in inhibiting SARS-CoV2, while not exhibiting toxicity at the concentrations tested.

In a separate *in vivo* model, the anti-miR-2392 FASTmer was evaluated in a Syrian hamster infection model (**Fig. 6H-6J**). Initially six hamsters were treated with FASTmers for 72 hours without infection to observe any changes in animal behavior indicating toxicity. There were no observed changes in animal behavior indicating a lack of obvious toxicity. Following this study, 30 male hamsters were divided into 5 treatment groups. The infected hamsters were given  $10^5$  plaque forming units (pfu) of WA01/2020 strain of SARS-CoV-2 passaged twice in Vero E6 cells from the original isolate obtained from BEI Resources. The anti-miR-2392 FASTmer treatment was given by intraperitoneal (IP) injection or intranasal (IN) instillation 24 hours before viral inoculation or both 24 hours before and 24 hours after viral inoculation. Each

FASTmer dose was at a concentration of 10  $\mu$ M in a 100  $\mu$ L volume (approximately 0.13 mg/kg). Half of the hamsters in each group ( $n = 3$ ) were euthanized and necropsied on day 3 and 7 post-infection respectively.

Loss of body weight of hamsters over the course of the experiment were  $<10\%$  in all groups and significantly different for the IN treatment one day before viral inoculation (compared to the control) and while statistical differences between other groups were not present (**Fig. 6H**). Virus titers from oropharyngeal swabs of hamsters receiving IN treatment were significantly lower ( $p = 0.018$ ) than those from hamsters receiving FASTmers IP or PBS on day 1 post-challenge, but there were no differences among groups in magnitude of shedding on days 2 and 3 post-challenge (**Fig. 6I**). Although not statistically different than the control treatment, the data indicates a downward trend with FASTmer treatment (**Fig. 6J**). In addition, the total histopathological score for the IN was lower than the controls although not significant.

#### *The impact of miR-2392 on diseases, relationship to COVID-19 symptoms, and predicted FDA drugs to target miR-2392*

To predict whether miR-2392 might have a direct relationship to COVID-19 symptoms in the host, we determined the pathway and disease relevance of miR-2392 using miRnet (Chang et al., 2020b). Among the diseases predicted to be associated with miR-2392 were a surprising number of clinical observations present in individuals with COVID-19 infection (**Fig. 7A**). These include heart or cardiovascular disease and failure, both known to heavily contribute to morbidity and mortality in patients with COVID-19 (Nishiga et al., 2020), hyperesthesia (Krajewski et al., 2021), as well as less common COVID-19 symptoms, such as lymphadenopathy and pharyngitis related to sore throat (Edmonds et al., 2021; Walsh-Messinger et al., 2020), liver dysfunction (Portincasa et al., 2020), splenomegaly (Malik et al., 2020), CNS (Mahajan and Mason, 2021; Rodriguez et al., 2020) and kidney failure (Hultstrom et al., 2021).

It is interesting to note that miR-2392 was also predicted to affect diseases that appeared not to be associated with COVID-19 infection, but literature searches reveal these pathologies do occur in some COVID-19 patients. For example, azoospermia, which is linked to male infertility, has been shown to occur in some male patients (Younis et al., 2020). The menstrual cycle in females have been reported to be deregulated for months after COVID-19 infection (Li et al., 2021). Association with dental damage has also been observed in COVID-19 patients (Sirin and Ozcelik, 2021), also deafness or hearing loss (Koumpa et al., 2020). We used the tool Kaplan-Meier Plotter (Nagy et al., 2018) to associate miR-2392 expression with pan-cancer patient survival (**Fig. S7**). We observed that the high expression of miR-2392 is generally related to poor prognosis with the majority of cancer types ( $p\text{-value} < 0.05$ ). If miR-2392 is associated with COVID-19, as we are hypothesizing, and is persistent after the virus clears the host, then the implications for the potential long-term impact on the millions of people infected with COVID-19 could be devastating. Intriguingly, one of the miR-2392 predicted consequences in the immune category is decreased antibody levels in the blood; this might account for the reported loss of the antibodies overtime (Gudbjartsson et al., 2020; Self et al., 2020).

Using computational prediction models, we also predicted small molecules, including FDA-approved drugs that could inhibit miR-2392 from two different approaches. The first approach employed a state-of-the-art machine learning method that we recently developed for predicting

missing drug targets (Galeano et al., 2021). We applied this algorithm on an association dataset between 213 small molecules and 1,519 miRNAs from the SM2miR database (Liu et al., 2013) (see statistics in **Fig. S8**). Our model also integrated chemical similarity between small molecules and sequence similarity between miRNAs. In ten-fold cross-validation experiments, we achieved an average area under the receiver operating curve of 0.877 when predicting missing small molecule-miRNA associations (**Fig. S9**). A list of the top-20 predicted small molecules for miR-2392 (**Fig. 7B**) includes Dexamethasone, the first drug known to save lives in critically ill COVID-19 patients (Ledford, 2020), and Atorvastatin, that has shown similar protective role in COVID-19 patients (Rossi et al., 2020). The second approach follows ideas first presented in Sirota *et al.* (Sirota et al., 2011) and consists on analyzing the genomic signature of miR-2392 (*i.e.* significant up and down-regulated genes) and predicting small molecules that can reverse it. We screened the genomic signature of miR-2392 against the genomic signature of 30,000 small molecules contained in the connectivity map (CMAP) (Lamb et al., 2006). The top-20 small molecules predicted by our approach (Sirota et al., 2011) includes the androgen receptor antagonist Enzalutamide and the insulin sensitizer Pioglitazone (Carboni et al., 2020) both of which are in clinical trials for COVID-19 (**Fig. 7C**; Clinical Trial #NCT04475601 and NCT04604223). We also found literature evidence for the leukotriene inhibitor ubenimex (Asai et al., 2020), and the bacterial DNA inhibitor metronidazole (Gharebaghi et al., 2020).

## Discussion

While the potential eradication of the novel coronavirus through worldwide vaccination is underway, there remains a major need to develop effective interventional strategies to minimize the damage caused by coronavirus infections. Host-mediated lung inflammation is a driver of mortality in COVID-19 critically ill patients. Thus, it is logical to focus on therapeutics that may have immunomodulating properties or disrupt viral replication. Our research uncovers a novel eight miRNA signature in patients with COVID-19 viral loads compared to those without disease as predicted from RNA-seq data. The expression of seven miRNAs was decreased (miR-10, miR-1, miR-34a-5p, miR-30c-5p, miR-29b-3p, miR-124-3p, and miR-155-5p) while a single miRNA, miR-2392, was significantly increased (**Fig. 1**). This key miRNA signature was involved in major cellular and molecular mechanisms that drives the viral-host response.

From previous research, the upregulation of miR-10a-5p, from the miR-10 precursor miRNA, provides antiviral benefits through the suppression of SDC1 that can act as a defense mechanism for Porcine hemagglutinating encephalomyelitis viruses (Hu et al., 2020). The upregulation of miR-124 is shown to inhibit the Japanese encephalitis virus replication (Yang et al., 2016). Notably, the upregulation of miR-30c-5p and miR-155-5p have been independently shown to be involved with antiviral functions through immune and inflammatory pathways with other type of coronaviruses (Dickey et al., 2016; Ma et al., 2018). It was also indicated that inhibition of miR-34a-5p in the host by SARS-CoV-2 suppresses beneficial antiviral pathways that this miRNA regulates. (Bartoszewski et al., 2020; Sacar Demirci and Adan, 2020). miR-1-3p has previously been identified as an antiviral agent for viral related respiratory diseases and the downregulation by SARS-CoV-2 is predicted to follow similar pathways for survival in the host (Sardar et al., 2020). Examination of patients with COVID-19 showed increased levels of miR-2392 circulating blood (**Fig. 5**). Interestingly, we show that for both miR-1-3p and miR-155-5p



from serum patient samples were significantly inhibited (**Figs. S3 and S4**), which is in agreement with the current viral literature as discussed above. MiR-124-3p was shown to have no significant changes and barely present for SARS-CoV-2 patients (**Fig. S5**), indicating the responses discussed above is potentially specific for Japanese encephalitis virus.

Several studies have measured differential expression of miRNAs in COVID-19 patients and proposed their use as biomarkers or therapeutics. A post-mortem examination from lung biopsies in nine COVID-19 patients compared to controls found miR-26a, miR-29b, and miR-34a were correlated to endothelial dysfunction and inflammatory biomarkers (Centa et al., 2020). In a separate study performing multi-transcriptome sequencing in red blood cell depleted whole blood from moderate or severe COVID-19 patients four additional miRNAs, miR-146a, miR-21, miR-142, and miR-15b, were identified as potential biomarkers as well as contributors to disease pathogenesis (Tang et al., 2020). It has also been suggested to use miRNAs to target the angiotensin-converting enzyme 2 (ACE2) receptor that facilitates endocytosis of viral particles into the cells to limit virus-induced glomerular injury, cell infection, kidney damage (Mishra et al., 2020; Nersisyan et al., 2020; Pontecorvi et al., 2020; Sacar Demirci and Adan, 2020; Sardar et al., 2020; Teodori et al., 2020; Widiasta et al., 2020). While these studies are limited to a specific tissue, our data that correlates miRNA signatures from multiple tissues (**Fig. 3**) suggests miR-2392 is a unique target that is ubiquitously involved in COVID-19 symptoms.

In 2010, miR-2392 was found in a small-RNA deep-sequencing of normal and malignant human B-cells where it was altered among hundreds of other microRNAs (Jima et al., 2010). Since then, the majority of publications with miR-2392 are focused on cancer tissues and have found a potential role for miR-2392 in driving cellular invasion and metastasis through an epithelial-mesenchymal transition. In 2013, miR-2392 was one of 6 circulating microRNAs altered in the serum and tissue of patients with cervical squamous cell carcinoma that was used to predict the occurrence of lymph node metastasis with the potential to assist in clinical staging (Chen et al., 2013). Higher levels of miR-2392 in gastric cancer was found to be associated with lower clinical staging and increased patient survival (Li et al., 2017). It was shown that miR-2392 inhibited gastric cell invasion and metastasis by targeting MAML3 and WHSC1 for degradation that subsequently decreased an epithelial-mesenchymal transition through the loss of Snail1, Slug, and Twist1 expression. Similarly, miR-2392 and miR-1587 were found to target the ZEB2 protein, a promoter of the epithelial-mesenchymal transition. A lower expression of these two miRNAs were found in human keloid tissues that resulted in a loss of inhibition of ZEB2 and subsequent promotion of cellular proliferation and invasion in keloids (Hou et al., 2019). Inhibition of miR-2392 by the long-non-coding RNA CACNA1G-AS1 was found to promote hepatocellular carcinoma through disrupting the degradation of C1orf61, a tumor activator associated with metastasis and tumor progression (Hu et al., 2013; Yang et al., 2019). Recently, Fan et al. demonstrated a novel role for miR-2392 in the regulation of chemoresistance in tongue squamous cell carcinoma by partial inhibition of mitochondrial DNA (mtDNA) transcription through direct miRNA-mtDNA base pairing which resulted in reprogramming tumor cell metabolism (Fan et al., 2019). These reports for miR-2392 establish the significant impact this single miRNA may have in on cellular activity. Particularly relevant to this study was the altered expression of miR-2392 found in Hepatitis B viral infections. Its expression was found to be increased by more than 2-fold in extracellular vesicles secreted from human hepatocytes infected



with the Hepatitis B virus (Enomoto et al., 2017). While miR-2392 has a reported impact on tumor cell biology, our study expands the valuable therapeutic potential of targeting miR-2392 to subsequently decrease SARS-CoV-2 viral infections (**Fig. 6**). These results warrant further exploration of the mechanistic underpinnings for the role of miR-2392 in driving viral infection.

One therapeutic insight deduced from miR-2392 interactions is the importance of the mitochondrial oxidative phosphorylation (OXPHOS) and glycolytic pathways in COVID-19, dramatically highlighted in BALF samples reported in **Fig. 1C**. In a study of tongue squamous cell carcinoma (Fan et al., 2019) it was reported that miR-2392 enters the mitochondrion where it binds to Ago2 and then binds to nucleotides 4379 to 4401 in the mtDNA heavy (H) strand. This binding site is within the MT-TQ (tRNA glutamine) gene, which encompasses nucleotides m.4329-4400. MT-TQ is part of a large polycistronic transcript transcribed from the H-strand promoter. This transcript encompasses 12 of the mtDNA H strand polypeptide genes punctuated by tRNAs. Cleavage of the tRNAs releases the mRNAs. Up-stream of MT-TQ are the 12S and 16S rRNAs and the complex I gene MT-ND1 gene. Downstream of MT-TQ is MT-ND2, MT-CO1, MT-CO2, MT-ATP6/8, MT-ND3, MT-ND4L, MT-ND4, MT-ND5, and MT-CYB (Lott et al., 2013; Wallace, 2018). Strikingly, the down-regulated mtDNA genes from the BALFS are the complex IV (cytochrome c oxidase) genes MT-CO1 and MT-CO2, the complex III (the bc<sub>1</sub> complex) gene (MT-CYB), and the complex I genes (MT-ND2, MT-ND4, and MT-ND5) (**Fig. 1C** right side arc). Since the miR-2392 inhibition of mtDNA OXPHOS genes shown for the BALF samples (**Fig. 1C**) is also reflected in the miR-2392 down-regulation of the nuclear DNA coded mitochondrial transcripts of the complex I and IV genes and the iron-sulfur and heme iron complexes in the nasal, heart, and kidney autopsy samples (**Fig. 3D**), mitochondrial inhibition by miR-2392 appears to be the only physiological function that is common across all tissues in infected individuals. This suggests that mitochondrial modulation is a central feature of SARS-CoV-2 pathophysiology.

The inhibition of mitochondrial genes by miR-2392 would impair OXPHOS, which would have the most adverse effects on the high mitochondrial energetic tissues (brain, heart, kidney), the tissues central to the most severe COVID-19 cases. Inhibition of mitochondrial OXPHOS genes would increase mitochondrial reactive oxygen species (mROS) production, and induce glycolysis to compensate for the energy deficit (see top of **Fig 1C**). Mitochondrial function is regulated by the Sirtuins (Carrico et al., 2018), mitochondrial decline is associated with senescence, and mROS oxidation of mtDNA is linked to activation of the inflammasome and thus NFκB (West et al., 2015; West and Shadel, 2017; Zhong et al., 2018), all of which are modulated around miR-2392 (**Fig. 1C**). Thus, SARS-CoV-2 induction of miR-2392 (**Fig. 5**) and its associated inhibition of mtDNA and nuclear DNA OXPHOS genes (**Fig. 3** and **S1**) could explain many of the metabolic disturbances of COVID-19. Conversely, antagonism of miR-2392 function should ameliorate the inhibition of OXPHOS and may explain the therapeutic benefit of the anti-miR-2392 FASTmers.

Using miRNAs from serum as a biomarker was first established in patients for the examination of diffuse large B-cell lymphoma (Lawrie et al., 2008). The use of miRNAs as a diagnostic biomarker has several advantages. Circulating miRNAs are readily obtained through a minimally invasive blood draw and are remarkably resistant to degradation in the plasma and serum (Mitchell et al., 2008). Measuring differentially expressed miRNAs may also provide a

means to detect asymptomatic individuals as previously demonstrated in another viral infection (Hou et al., 2017). However, potential confounding diseases that may influence the expression of multiple miRNAs requires the further evaluation of the targets found in this study (**Fig. 5**).

Recent advances in RNA chemistry and delivery systems enabled the first miRNA-based agents to enter into clinical trials several years ago (Rupaimoole and Slack, 2017). It was discovered that miR-122 increased the stability and replication of the Hepatitis C virus (HCV) through binding to the 5' end of the non-coding region that prevented degradation by the Xrn1 exoribonuclease (Jopling et al., 2005; Thibault et al., 2015). In a phase I clinical trial, a 15-nucleotide phosphorothioate DNA-locked nucleic acid anti-miRNA that is designed to inhibit miR-122 was first used and demonstrated no adverse reactions. In a subsequent phase IIa trial of 36 patients, there was a significant dose-dependent decrease in HCV load, one patient reported a grade 3 adverse event (thrombocytopenia), and only a small set of patients experienced viral rebound that may be linked to mutations of the HCV viral RNA (Janssen et al., 2013; Ottosen et al., 2015). A separate clinical trial with a N-acetyl-Dgalactosamine (GalNAc)-conjugated anti-miRNA targeting miR-122 and antiviral agents (ledipasvir and sofosbuvir) was successful in reducing viral loads in all treated patients within 4 weeks of treatment as well as sustained viral response in three patients after 76 weeks of follow-up (van der Ree et al., 2017), however subsequent treatments have been suspended due to two cases of severe jaundice. These clinical trials have demonstrated the promising potential of using anti-miRNAs to significantly reduce viral infection with limited adverse effects and the similarities with miR-2392 with SARS-CoV-2 warrant further investigations to push to clinical trials.

Presently, there remains no specific treatment option for patients presenting with severe COVID-19 disease. While vaccines provide a promising avenue towards preventing the development of these symptoms as well as curbing the infection rate, there remains an urgency to successfully develop and implement therapeutic agents to reduce severe consequences from infection and subsequent patient mortality. As the testing of antibody-based or drug targeted therapies are currently underway, the added utility of miRNAs represents a novel category of therapeutic agents that have previously shown endogenous activity to alter viral infection.

**Acknowledgments:** This work was supported by supplemental funds for COVID-19 research from Translational Research Institute of Space Health through NASA Cooperative Agreement NNX16AO69A (T-0404 to A.B. and T-0406 to A.C.) and further funding from KBR, Inc provided to A.B; this work used resources services, and support provided via the COVID-19 HPC Consortium (<https://covid19-hpc-consortium.org/>) which is a unique private-public effort to bring together government, industry, and academic leaders who are volunteering free compute time and resources, in support of COVID-19 research and resources supporting this work were provided by the NASA High-End Computing (HEC) Program through the NASA Advanced Supercomputing (NAS) Division at Ames Research Center which was awarded to A.B.; DOD W81XWH-21-1-0128 awarded to D.C.W.; NIGMS P20 GM1009005 awarded to N.A.; Individual National Research Service Award F32-AI147587 awarded to J.M.D.; NIH/NHBLI K08 HL143271 and NIH/NHLBI R03 HL155249 awarded to R.S.H.; NIH/NCI U54 CA260543 supported R.S.H., N.M.B., M.C.W.; NSF 1956233 awarded to R.M.; A.P. was supported by Biotechnology and Biological Sciences Research Council (<https://bbsrc.ukri.org/>) grants BB/K004131/1, BB/F00964X/1 and BB/M025047/1, Consejo Nacional de Ciencia y Tecnología

Paraguay - CONACyT (<http://www.conacyt.gov.py/>) grants 14-INV-088 and PINV15-315, National Science Foundation Advances in Bio Informatics (<https://www.nsf.gov/>) grant 1660648; D.G. and A.P. were supported by the CONACyT grant PINV20-337 and the Fundação Getulio Vargas. N.M.B. was supported by the National Center for Advancing Translational Sciences (NCATS), NIH UL1TR002489, 2KR1272005, 550KR242003. Thanks to Dr. Richard Bowen for his assistance with the hamster studies.

## Author contributions

Conceptualization: A.B.; Methodology: A.B.; Formal Analysis: A.B., R.M., C.V., D.T., F.J.E., C.M., C.M., J.C.S., J.T.M., J.M.D., D.G., U.S., E.S.W., A.S., J.F., V.Z., N.S., T.J.T.; Investigation: A.B., C.V., R.M., C.E.M., A.C., P.N., M.F., R.A.B., M.M., S.L.M., A.Y., T.R.A.; Sample Collection: M.M.S., M.C.W., R.S.H., N.M.B., U.C.P.C., A.D.H., J.C.; Resources: A.B., R.M., C.E.M., A.C., M.S., M.F., M.C.W.; Writing – Original Draft: A.B., J.T.M.; Writing – Review & Editing: A.B., J.T.M., F.J.E., R.J.G., W.P., M.M.S., J.M.D., J.W.G., D.W., S.B., V.Z., E.S.W., S.V.C., N.A., A.P., D.G., M.F., P.M.C., M.M., M.R.E., J.C.S., A.C., R.M., N.S., T.J.T., B.C., L.N.S., M.C.W.; Visualization: A.B., J.S.C., F.J.E., D.G., N.S., V.Z.; Supervision: A.B.; Funding Acquisition: A.B.

## Declaration of Interests

The authors declare no competing interests.

## Figure Legends

**Figure 1. Key miRNA signature as predicted from Bronchial Alveolar Lavage Fluid (BALF) RNA-seq data in patients with COVID-19.** **A)** Predicted upstream regulators determined through Ingenuity Pathway Analysis (IPA) consistent with the transcriptional response from differentially expressed genes (FDR<0.05; outer ring). Eight miRNAs were among the key regulators in response to COVID-19 (inner ring). **B)** Major biological responses resulting from dysregulation of this eight miRNA signature drive immune- and inflammatory-related pathways as well as mitochondrial dysfunction determined through IPA. **C)** Pathway regulation by miR-2392 from BALF RNA-seq data determined through IPA.

**Figure 2. Cross-species and viral integration of miR-2392.** **A)** The conservation of miR-2392 across species determined by UCSC Genome Browser. The boxes (■) represent aligning and conserved sequence regions. Double horizontal line (=) represents both the genome and query have unalignable sequence between regions of aligned sequence, a double-sided insertion. Single lines (-) indicate gaps that are largely due to a deletion in the genome of the first species or an insertion in the genome of the second species. **B)** The expression of MEG3, the miR-2392 host gene, in different tissues from healthy patients. **C)** Potential binding sites of miR-2392 visualized across 300 windows of 100bp length in SARS-CoV-2 genomes (NC045512.2 reference, and representative genomes for variants and lineages of concern from GISAID). The score in each window is the average of miRanda scores for hits within that 100bp window. Three top hits are shown explicitly at the bottom of the plot.

**Figure 3. Gene targets of miR-2392 in COVID-19 patients as well as mitochondrial and inflammatory genes.** Volcano plots showing the differential gene expression analysis from **A)** nasopharyngeal swab and autopsy COVID-19 patient tissues from the **B)** heart, **C)** kidney, **D)** liver, **E)** lung, and **F)** lymph node from RNA-seq datasets separated by viral load. **G)** Differential gene expression analysis for all miR-2392 gene targets significantly expressed in nasopharyngeal swab and autopsy COVID-19 patient tissues. The heatmaps display the t-score statistics for comparing viral load vs negative patient sample for all samples. Main gene clusters were determined through k-mean clustering. Six main gene clusters were determined and ShinyGO (Ge et al., 2020) was utilized to determine the pathways for each cluster which are displayed on the top panel of the heatmap. miR-2392 gene targets in for **H)** mitochondrial specific genes or **I)** inflammatory genes are displayed. Differentially expressed genes are shown with at least one comparison demonstrating a significant adjusted p-value ( $FDR < 0.05$ ) when comparing COVID-19 patients (high, medium or low viral loads) to non-infected control patients (none). A heatmap for the miR-2392 mitochondrial gene targets from the full list of targets determined only from miRmap is available in **Fig. S1**. A heatmap for the miR-2392 inflammatory gene targets from the full list of targets determined only from miRmap is available in **Fig. S2**. **J)** Scatter plot of  $\log_2$ -transformed Fold Changes in RNAs and proteins for miR-2392 targets. The chart shows a set of genes differentially expressed at the RNA level. Student's t-test, RNA p-value  $\leq 0.05$ , no limitation on protein p-value. **K)** Scatter plot of  $\log_2$  transformed medians in RNAs and proteins. The orange color represents COVID-19 positive samples, grey - COVID-19 negative samples. Student's t-test is used in Fold Change calculations. The size and the opacity of the point represent  $\log_2$ -transformed Fold Change at the RNA level. The shape of the point represents Fold Change direction: circle - positive, triangle - negative. Pearson correlation for COVID-19 positive samples displayed in orange, for COVID-19 negative samples - in grey.

**Figure 4. Increased miR-2392 expression *in vitro* mimics a COVID-19 disease phenotype.** **A-F)** Volcano plots for RNA-seq results in cells overexpressing miR-2392. **G-J)** Correlation plot of RNA-seq between miR-2392 overexpression and related SARS-CoV-2 datasets. The circle size is proportional to the correlation coefficient. Statistical significance was determined using a two-tailed Student's t-test  $*p < 0.05$ ,  $**p < 0.01$ ,  $***p < 0.001$ . **K-O)** Dot plots for statistically significant gene sets determined by fGSEA. NES, nominal enrichment score. **P)** and **Q)** Predicted miR-2392 targets by the MIRDIP algorithm that are downregulated in the overexpression experiments. The putative miR-2392 mRNA targets belonging to the consensus transcriptomic networks observed in SARS-CoV-2, MERS and Influenza infections of different human cells are represented in a Venn diagram in the upper part of the panel **P**.

**Figure 5. Circulating miR-2392 with COVID-19 patients compared to COVID-19 negative patients.** Droplet digital PCR (ddPCR) with specific primer for miR-2392 was performed on serum, urine, and nasopharyngeal swab samples (including other seasonal coronavirus samples) from COVID-19 positive and negative patients. The miRNA concentration is reported as copies/5ng RNA. **A)** The levels of miRNA-2392 in all tissues from patients grouped as SARS-CoV-2 positive (SARS-nCoV-2) or negative (neg). Unadjusted t-tests comparing the SARS-CoV-2 positive to neg for each tissue are provided and also adjusted statistics comparing the



groups with a mixed model corrected for age and sex is provided. **B)** Receiver Operating Characteristic (ROC) curve is provided for miR-2392 for each tissue comparing SARS-CoV-2 positive to negative patients. **C)** Comparing specific categories within each tissue type between COVID-19 positive and negative patients. N = COVID-19 Negative, P = COVID-19 positive, P<sub>int</sub> = intubated patients, outp = outpatient, ICU = Intensive care unit/inpatient, Cold = Coronaviruses related to the common cold, NL63 = NL63 coronavirus, and CoV-2 = SARS-CoV-2. For all plots \* = p < 0.05, \*\* = p < 0.01, and \*\*\* = p < 0.001. We also quantified three other miRNAs with same patient samples as comparison which were miR-1-3p (**Fig. S3**), miR-155-5p (**Fig. S4**), and miR-124-3p (**Fig. S5**).

**Figure 6. Anti-miR-2393 therapeutic mitigation of SARS-CoV-2 infection with *in vitro* and *in vivo* models.** **A)** Schematic of the design for the miR-2392 inhibitor with the FASTmer platform, the synthesis and formulation of the inhibitor, and the experimental models utilized for testing the inhibitor. **B) – D)** Anti-miR-2392 FASTmer inhibitor applied to A549 human cells infected with SARS-CoV-2 and tested for viral viability and cytotoxicity. Viral viability is inhibited by 100% with near 0% cytotoxicity. **E) – G)** Nonsense FASTmer inhibitor applied to A549 human cells infected with SARS-CoV-2 and tested for viral viability and cytotoxicity. Viral viability is inhibited by 50% with near 0% cytotoxicity. **H) – J)** Toxicity and efficacy of anti-miR-2392 FASTmer inhibitor in an *in vivo* infection hamster model. There were six treatments groups: SBCov207 by IP injection 24 hours prior to viral inoculation (IP Day -1), SBCov207 by IP injection 24 hours prior to viral inoculation and 24 hours post-viral challenge (IP Day -1, +1), SBCov207 by IN injection 24 hours prior viral inoculation (IN Day -1), SBCov207 by IN injection 24 hours prior viral inoculation and 24 hours post-viral challenge (IN Day -1, +1), and 100ul of PBS as a control treatment 24 hours prior and post-viral challenge through IN instillation (PBS IN Day -1, +1). **H)** Weights per day for each of the 5 groups pooled (n = 6 for days 1 – 3 and n = 3 for days 4 -7), and the maximum percent weight loss, observing for the two different endpoints. **I)** SARS-CoV-2 assayed by plaque assay on Vero E6 cells from oropharyngeal swabs collected on days 1, 2 and 3. N=6 for each treatment group. **J)** Histopathological total score for lung tissues at day 3; anti-miR-2392 treatments have lower scores than the PBS control. Intranasal (IN), intraperitoneal (IP).

**Figure 7. Predicted impact of miR-2392 on human disease and the top-20 drug compounds predicted to affect miR-2392 expression through machine learning approach.** **A)** Dot plot of diseases associated with miR-2392, as predicted from miR-2392 gene targets by miRnet. The diseases were manually curated to emphasize specific diseases and tissues. The values are plotted according to p-value, and the size of each dot represents the number of downstream gene targets for miR-2392 associated with each disease prediction. The specific cancer relationship to miR-2392 is highlighted in **Fig. S7**, relating miR-2392 expression with patient survival in a pan-cancer analysis. **B)** Barplot of scores using our matrix completion model to predict small molecules that affect miRNA expression. Higher scores indicate more predicted associations. **C)** Barplot of the normalized connectivity map (CMAP) scores. We used transcripts induced by miR-2392 overrepresented genes to query CMAP. Higher negative scores reflect a greater



reversal of the miR-2392 transcriptomic signature. Further details on model statistics and performance are found in **Figs. S8 – S10**.

## Supplemental Figures and Material

### The UNC COVID-19 Pathobiology Consortium is comprised of:

Shannon M Wallet<sup>1,2</sup>, Robert Maile<sup>2,3</sup>, Matthew C Wolfgang<sup>2,4</sup>, Robert S Hagan<sup>4,5</sup>, Jason R Mock<sup>4,5</sup>, Natalie M Bowman<sup>6</sup>, Jose L Torres-Castillo<sup>5</sup>, Miriya K Love<sup>5</sup>, Suzanne L Meinig<sup>4</sup>, Will Lovell<sup>1</sup>, Colleen Rice<sup>5</sup>, Olivia Mitchem<sup>1</sup>, Dominique Burgess<sup>1</sup>, Jessica Suggs<sup>1</sup>, Jordan Jacobs<sup>3</sup>

<sup>1</sup>Department of Oral and Craniofacial Health Sciences, UNC Adams School of Dentistry, University of North Carolina School of Medicine, Chapel Hill, NC, 27599, USA

<sup>2</sup>Department of Microbiology & Immunology, University of North Carolina School of Medicine, Chapel Hill, NC, 27599, USA

<sup>3</sup>Department of Surgery, University of North Carolina School of Medicine, Chapel Hill, NC, 27599, USA

<sup>4</sup>Marsico Lung Institute, University of North Carolina at Chapel Hill, Chapel Hill, NC, 27599, USA

<sup>5</sup>Division of Pulmonary Diseases and Critical Care Medicine, Department of Medicine, University of North Carolina, Chapel Hill, NC 27599, USA

<sup>6</sup>Division of Infectious Disease, School of Medicine, University of North Carolina, Chapel Hill, NC, 27599, USA

**Figure S1. Mitochondrial gene targets of miR-2392 and regulated pathways. Related to Figure 3.** Differential gene expression analysis for all miR-2392 mitochondrial gene targets significantly expressed in nasopharyngeal swab and autopsy COVID-19 patient tissues. The heatmaps display the t-score statistics for comparing viral load vs negative patient sample for all samples. Main gene clusters were determined through k-mean clustering. Nine main gene clusters were determined and ShinyGO (Ge et al., 2020) was utilized to determine the pathways for each cluster which are displayed on the top panel of the heatmap. Differentially expressed genes are shown with at least one comparison demonstrating a significant adjusted p-value (FDR<0.05) when comparing COVID-19 patients (high, medium or low viral loads) to non-infected control patients (none). Mir-2392 gene targets only determined from miRmap.

**Figure S2. Inflammatory gene targets of miR-2392 and regulated pathways. Related to Figure 3.** Differential gene expression analysis for all miR-2392 inflammatory gene targets significantly expressed in nasopharyngeal swab and autopsy COVID-19 patient tissues. The heatmaps display the t-score statistics for comparing viral load vs negative patient sample for all samples. Main gene clusters were determined through k-mean clustering. Eight main gene clusters were determined and ShinyGO (Ge et al., 2020) was utilized to determine the pathways for each cluster which are displayed on the top panel of the heatmap. Differentially expressed genes are shown with at least one comparison demonstrating a significant adjusted p-value

(FDR<0.05) when comparing COVID-19 patients (high, medium or low viral loads) to non-infected control patients (none). Mir-2392 gene targets only determined from miRmap.

**Figure S3. Circulating miR-1-3p with COVID-19 patients compared to COVID-19 negative patients. Related to Figure 5.** Droplet digital PCR (ddPCR) with specific primer for miR-1-3p was performed on serum, urine, and nasopharyngeal swab samples (including other seasonal coronavirus samples) from COVID-19 positive and negative patients. The miRNA concentration are reported as copies/5ng RNA. **A)** The levels of miRNA-2392 in all tissues from patients grouped as SARS-CoV-2 positive (SARS-nCoV-2) or negative (neg). Unadjusted t-tests comparing the SARS-CoV-2 positive to neg for each tissue are provided and also adjusted statistics comparing the groups with a mixed model corrected for age and sex is provided. **B)** Receiver Operating Characteristic (ROC) curve is provided for miR-1-3p for each tissue comparing SARS-CoV-2 positive to negative patients. **C)** Comparing specific categories within each tissue type between COVID-19 positive and negative patients. N = COVID-19 Negative, P = COVID-19 positive, P<sub>int</sub> = intubated patients, outp = outpatient, ICU = Intensive care unit/inpatient, Cold = Coronaviruses related to the common cold, NL63 = NL63 coronavirus, and CoV-2 = SARS-CoV-2. For all plots \* = p < 0.05, \*\* = p < 0.01, and \*\*\* = p < 0.001.

**Figure S4. Circulating miR-155-5p with COVID-19 patients compared to COVID-19 negative patients. Related to Figure 5.** Droplet digital PCR (ddPCR) with specific primer for miR-155-5p was performed on serum, urine, and nasopharyngeal swab samples (including other seasonal coronavirus samples) from COVID-19 positive and negative patients. The miRNA concentration are reported as copies/5ng RNA. **A)** The levels of miRNA-2392 in all tissues from patients grouped as SARS-CoV-2 positive (SARS-nCoV-2) or negative (neg). Unadjusted t-tests comparing the SARS-CoV-2 positive to neg for each tissue are provided and also adjusted statistics comparing the groups with a mixed model corrected for age and sex is provided. **B)** Receiver Operating Characteristic (ROC) curve is provided for miR-155-5p for each tissue comparing SARS-CoV-2 positive to negative patients. **C)** Comparing specific categories within each tissue type between COVID-19 positive and negative patients. N = COVID-19 Negative, P = COVID-19 positive, P<sub>int</sub> = intubated patients, outp = outpatient, ICU = Intensive care unit/inpatient, Cold = Coronaviruses related to the common cold, NL63 = NL63 coronavirus, and CoV-2 = SARS-CoV-2. For all plots \* = p < 0.05, \*\* = p < 0.01, and \*\*\* = p < 0.001.

**Figure S5. Circulating miR-124-3p with COVID-19 patients compared to COVID-19 negative patients. Related to Figure 5.** Droplet digital PCR (ddPCR) with specific primer for miR-124-3p was performed on serum, urine, and nasopharyngeal swab samples (including other seasonal coronavirus samples) from COVID-19 positive and negative patients. The miRNA concentration are reported as copies/5ng RNA. For miR-124-3p, the copies/5ng were either equal to 0 or at extremely low levels close to 0 copies/5ng. To try to determine any statistical differences we categorized the groups as ND = Not Determined which are all 0 values or D = Determined which are values > 0 for both N = negative (open symbols) and P = COVID-19 positive patients samples (closed symbols). The number of patients for each column is shown

above the points. No significant differences were observed for any of the sample for miR-124-3p.

**Figure S6. miR-2392 expression pan-cancer survival analysis. Related to Figure 7.** Kaplan Meier patient survival plots for miR-2392 expression in a pan-cancer analysis was determined utilizing The Kaplan Meier plotter (Nagy et al., 2021). The plots were separated with the top row being cancers which patients had significantly poor survival with high expression of miR-2392, the middle row being cancers which patients had poor survival (but not significant) with high expression of miR-2392, and the bottom row being cancers which patients had significantly better survival with high expression of miR-2392.

**Figure S7. Small molecules-miRNA dataset statistics Related to Figure 7.** (Left) Number of small molecules associated to miRNAs. (Right) Number of miRNAs associated to small molecules.

**Figure S8. Performance of our method at predicting missing small molecule-miRNA interactions. Related to Figure 7.** (Top) The mean value of the Receiver Operating Curve (ROC) is shown for a ten-fold cross-validation experiment (dark blue). 95% confidence interval is also shown (light blue). (Bottom) The mean value of the Precision-Recall Curve (PRC) is shown for a ten-fold cross-validation experiment (dark salmon). 95% confidence interval is also shown (light salmon).

**Figure S9. Performance of our method at predicting missing small molecule-miRNA interactions when controlling for data imbalance. Related to Figure 7.** (Top) Area Under the Receiver Operating Curve (AUROC) was obtained in a ten-fold cross-validation experiment for varying values of the negative to positive label ratio in the test set. (Bottom) Area Under the Precision-Recall Curve (AUROC) was obtained in a ten-fold cross-validation experiment for varying values of the negative to positive label ratio in the test set.

**Table S1. Annealing temperatures for miRNA primers, related to methods and Figure 5.** Temperatures used for droplet digital PCR to quantify each miRNA target.

## STAR Methods

## RESOURCE AVAILABILITY

### Lead Contact

Further information and requests for resources and reagents should be directed to and will be fulfilled by the Lead Contact, Afshin Beheshti ([afshin.beheshti@nasa.gov](mailto:afshin.beheshti@nasa.gov)).

### Materials Availability

This study did not generate new unique reagents.

### Data and Code Availability

The published article includes all datasets generated and analyzed during this study. Processed bulk RNA-seq data is available online (<https://covidgenes.weill.cornell.edu/>). RNA-Seq alignment script for BALF samples and SHSY-5Y cells studies are attached. Limma script for SHSY5Y studies is attached.

## EXPERIMENTAL MODEL AND SUBJECT DETAILS

### *Human serum and nasopharyngeal swab sample collection for ddPCR*

All plasma and nasal swab samples from those with COVID-19 infection, seasonal coronavirus infection, and controls were collected from inpatients at the University of Maryland Medical Center, in Baltimore, USA, between March and May of 2020. Sample collection obtained through informed consent waiver, which was approved by the University of Maryland, Baltimore IRB.

For serum samples, N=10 samples from COVID-19 intubated patients, COVID-19 outpatients, and COVID-19 negative patients were obtained. An equal distribution of N=5 males and females were used for each group. Also, an equal age distribution of patients from 27 to 85 years old was utilized for each group.

For the nasopharyngeal samples the following patient samples were obtained: N=10 SARS-CoV-2 positive patients, N=6 common cold coronavirus samples, and N=6 Coronavirus NL63 samples. For the common cold coronavirus samples the breakdown was the following for the specific viruses: N=2 Coronavirus 229E, Coronavirus HKU1, and N=2 Coronavirus OC43.

### *Human nasopharyngeal swab sample collection for RNA-seq analysis*

Patient specimens were processed as described in Butler et al., 2020 (Butler et al., 2021). Briefly, nasopharyngeal swabs were collected using the BD Universal Viral Transport Media system (Becton, Dickinson and Company, Franklin Lakes, NJ) from symptomatic patients. Total Nucleic Acid (TNA) was extracted from using automated nucleic acid extraction on the QIA Symphony and the DSP Virus/Pathogen Mini Kit (Qiagen).

### *Human autopsy tissue collection for RNA-seq analysis*

The full methods of the patient sample collection from the autopsy patients are currently available in the Park et al. (Park et al., 2021). All autopsies are performed with consent of next of kin and permission for retention and research use of tissue. Autopsies were performed in a negative pressure room with protective equipment including N-95 masks; brain and bone were not obtained for safety reasons. All fresh tissues were procured prior to fixation and directly into Trizol for downstream RNA extraction. Tissues were collected from lung, liver, lymph nodes, kidney, and the heart as consent permitted. For GeoMx, RNAscope, trichrome and histology tissue sections were fixed in 10% neutral buffered formalin for 48 hours before processing and sectioning. These cases had a post-mortem interval of less than 48 hours. For bulk RNA-seq tissues, post-mortem intervals ranged from less than 24 hours to 72 hours (with 2 exceptions - one at 4 and one at 7 days - but passing RNA quality metrics) with an average of 2.5 days. All deceased patient remains were refrigerated at 4°C prior to autopsy performance.



### ***Human urine sample collection***

Urine was collected from patients and volunteers at the University of North Carolina at Chapel Hill. All patients provided informed consent prior to participation in IRB-approved research protocols (UNC IRB: 20-0822 [RHS] and 20-0792 [NMB]). Mid-stream urine of outpatients and non-critically ill patients was collected by the clean catch method. Urine of intubated critically ill patients was collected from a port on the Foley catheter. Urine was aliquoted into 5 ml aliquots and stored at -80°C.

Urine aliquots were thawed, and microRNA was extracted from 1 ml per sample using Norgen Urine microRNA Purification Kit (Cat. 29000). Microalbumin and creatinine levels were assessed using Microalbumin 2-1 Combo strips (CLIAwaived Inc, cat# URS-2M).

### ***Cell lines used for miR-2392 mimic experiments***

Human SH-SY5Y cells were obtained from the ATCC and grown in Minimum Essential Medium (Gibco) / 10% FBS (Invitrogen) / 1% MEM Non Essential Amino Acids (Gibco) / 1% GlutaMAX -1 (Gibco). Cells were plated in 3.5 cm dishes and incubated with miR-2392 or control lentivirus particles (MOI 1) for 48h. Cells were harvested and lysed in Trizol reagent and RNA was extracted following manufacturers protocol (Invitrogen).

### ***COVID-19 hamster model***

Male Syrian hamsters 6-8 weeks old were utilized for efficacy studies with anti-miR-2392 FASTmer treatment. Three hamsters were used for each experimental group for a total of 30 hamsters with 10 treatment groups. Hamsters were infected with  $10^5$  pfu of SARS-CoV-2. There were 5 major treatment groups (N=6 per group) with two endpoints at day 3 or 7 post-viral challenge (N=3 per endpoint). Groups 1 and 3 were given the FASTmer treatment by IP injection while groups 2 and 4 were given by IN instillation under ketamine-xylazine anesthesia. Groups 1 and 2 were given single FASTmer treatment 24 hours before viral challenge. Groups 3 and 4 were given two doses of FASTmers at 24 hours before and 24 hours after viral challenge. The control group 5 was treated with PBS 24 hours prior to and 24 hours following viral challenge by IN instillation.

Treatment efficacy was assessed in multiple ways: 1) Change in daily body weight, 2) oropharyngeal shedding of virus on days 1-3 from all groups post-challenge assayed by plaque assay on Vero E6 cells (PFU/swab), 3) tissue burden of the virus at necropsy on day 3 from 2 lung tubes and turbinates assayed by plaque assay (PFU/100mg), and 4) histopathologic scoring on lungs and turbinates from all hamsters; the histopathological score for individual tissues, inflammation score from the interstitial lung inflammation, and total histopathological scores/assessment was made.

The dose of anti-miR-2392 that was used was calculated to raise blood levels to 10  $\mu$ M if it were given intravenously. The molecular weight of anti-miR-2392 is 15,804. Assuming that hamsters weigh 120 grams and have 8% of body weight as blood, blood volume was approximately 0.01 liters. The dose per hamster was 1.58 mg in a 100  $\mu$ l volume from an anti-miR-2392 solution.

# ***In vitro viral screening model***

A549-ACE2 cells, gifted by Dr. Brad Rosenberg (MSSM), were maintained in DMEM (Quality Biological, Gaithersburg, MD; #112-014-101) + 10% Fetal Bovine Serum (Gibco; #26140079) + 1% Penicillin-Streptomycin (Gemini Bio; #400-109). The day prior to treatment, 5,000 A549-ACE2 cells were plated per well in 96-well plates. MiR-2932 was diluted in duplicate in A549-ACE2 media to a starting concentration of 20μM (Run 1) or 22μM (Runs 2 and 3), and then an 8-point 1:2 dilution series was prepared. Media was removed from cells and 90μL of each dilution was transferred to the cells. The plates were incubated for 2 hours at 37°C before being infected with an M.O.I. of 0.1 SARS-CoV-2 WA-1 (provided by Dr. Natalie Thornburg at the Centers for Disease Control and Prevention). Parallel plates were also run and left uninfected to monitor toxicity. Since Runs 2 and 3 were run simultaneously, a single toxicity plate was run for both. All plates were incubated at 37°C for 72 hours before being analyzed via Cell Titer Glo (Promega, Madison, WI; #G7573). Cell viability was compared to uninfected, untreated cells and infected, untreated cells.

## **METHOD DETAILS**

### ***miRNA extraction for Droplet Digital PCR (ddPCR)***

MiRNA extractions from serum were carried out using the Qiagen miRNeasy serum/plasma kit (#217184). MiRNA extractions from urine samples were carried out using Norgen urine microRNA Purification Kit (Cat. 29000, Norgen Bioteck Corp. Thorold, ON, Canada). Quantitation of miRNA samples was done using a NanoDrop 2000 Spectrophotometer (ThermoFisher Scientific).

### ***cDNA generation and ddPCR***

First, cDNA was synthesized from miRNA samples using the Qiagen miRCURY LNA RT Kit (Cat. 339340) using a concentration of 5ng/μl for the miRNA per sample. Next, samples were mixed with a 1:20 dilution of the generated cDNA with the BioRad QX200 ddPCR Evagreen Supermix (Cat. 1864034) and the appropriate miRNA primers from miRCURY LNA miRNA PCR Assays (Qiagen). BioRad QX200 Automated Droplet Generator (Cat. 1864101) was used to create emulsion droplets. With the C1000 Touch™ Thermal Cycler with 96-Deep Well Reaction Module (Bio-Rad) the following PCR reaction was used for all the primers: 1 cycle 95°C for 5 min, 40 cycles of 95°C for 30 sec and 58°C for 1 min (the annealing temperature can change depending on the primer), 1 cycle of 4°C for 5 min, and 1 cycle of 90°C for 5 min. Not all miRNA primers sets for ddPCR will have the same annealing temperature, so optimizing the annealing temperature is required for each primer set. Their respective annealing temperatures are found in **Table S1**. Finally, the QX200™ Droplet Digital™ PCR System (Bio-Rad) quantified the amount of miRNA for each primer set per sample. QuantaSoft software (Bio-Rad) generated the data for each primer set and sample. The same threshold setting was used for all samples per primer set. The concentration (miRNA copies/μl) value generated by QuantaSoft was converted to miRNA copies/ng of serum. These values were used for all miRNA analysis. For all analysis the miRNA concentrations were  $\log_2(x+1)$  transformed to allow for easy comparison between miRNAs and samples.

# ***Publicly available Bronchial Alveolar Lavage Fluid (BALF) COVID-19 RNA-sequencing data***

Fastq files were downloaded from SRA (NCBI BioProject PRJNA605907 (Shen et al., 2020) and NCBI BioProject PRJNA390194 (Ren et al., 2018)). Fastq data files were trimmed using TrimGalore v (0.6.4) with a quality cutoff of 30. Data were then aligned using STAR (v2.7.3) two pass mode to the Human reference genome (GRCh38 v99 downloaded 04-27-2020). Unaligned data were written to a fastq file, and then realigned to the GRCh38 reference genome using Bowtie 2 (v2.3.4.1), and output sam file converted to a bam file using samtools (v1.7). The resultant Bam files were merged, sorted, and read groups added using picard tools (v2.21.3) (script in supplemental data).

# ***Publicly available RNA-seq data: A549, Calu-3, NHBE, and COVID-19 lung biopsy***

Raw RNA-seq read counts from the publication by Blanco-Melo *et al.* for the A549, Calu-3, and NHBE cell lines as well as post-mortem lung biopsies from two COVID-19 patients were downloaded from the Gene Expression Omnibus (series accession GSE147507) (Blanco-Melo et al., 2020).

# ***RNA-seq of Nasopharyngeal Swab COVID-19 patient samples***

RNA isolation and library preparation is fully described in Butler, et al. (Butler et al., 2021). Briefly, library preparation on the all nasopharyngeal swab samples' total nucleic acid (TNA) were treated with DNase 1 (Zymo Research, Catalog # E1010). Post-DNase digested samples were then put into the NEBNext rRNA depletion v2 (Human/Mouse/Rat), Ultra II Directional RNA (10 $\mu$ g), and Unique Dual Index Primer Pairs were used following the vendor protocols from New England Biolabs. Kits were supplied from a single manufacturer lot. Completed libraries were quantified by Qubit or equivalent and run on a Bioanalyzer or equivalent for size determination. Libraries were pooled and sent to the WCM Genomics Core or HudsonAlpha for final quantification by Qubit fluorometer (ThermoFisher Scientific), TapeStation 2200 (Agilent), and qRT-PCR using the Kapa Biosystems Illumina library quantification kit.

# ***RNA-seq of COVID-19 autopsy tissue samples***

RNA isolation and library preparation is fully described in Park, et al. (Park et al., 2021). Briefly, autopsy tissues were collected from lung, liver, lymph nodes, kidney, and the heart and were placed directly into Trizol, homogenized and then snap frozen in liquid nitrogen. At least after 24 hours these tissue samples were then processed via standard protocols to isolate RNA. New York Genome Center RNA sequencing libraries were prepared using the KAPA Hyper Library Preparation Kit + RiboErase, HMR (Roche) in accordance with manufacturer's recommendations. Briefly, 50-200ng of Total RNA were used for ribosomal depletion and fragmentation. Depleted RNA underwent first and second strand cDNA synthesis followed by adenylation, and ligation of unique dual indexed adapters. Libraries were amplified using 12 cycles of PCR and cleaned-up by magnetic bead purification. Final libraries were quantified using fluorescent-based assays including PicoGreen (Life Technologies) or Qubit Fluorometer (Invitrogen) and Fragment Analyzer (Advanced Analytics) and sequenced on a NovaSeq 6000 sequencer (v1 chemistry) with 2x150bp targeting 60M reads per sample.

# ***miR-2392 mimic experiments in SH-SY5Y cells and RNA-seq***

RNA was dissolved in nuclease free water and concentration determined spectrometrically at 260nm using a Biotek plate reader (Biotek). 500ng RNA was used as input for a whole transcriptome library preparation (ThermoFisher Total RNA). Libraries were quantified using a bioanalyzer chip reader (nanoDNA chips: Agilent Technologies) and diluted to 100 pM final concentration. Barcoded libraries were combined and use to seed a OneTouch bead templating reaction (OneTouch2). Cloned libraries were enriched and loaded on 540 Ion Torrent chips. Data were sequenced using the Ion Torrent RNA-seq workflow. Unaligned Bam files were converted to fastq and aligned to the Grch 38 reference genome using STAR Two pass approach (Dobin paper) to create gene count tables as described in Overberry et al. (Overbey et al., 2021) (script in supplementary).

## ***Anti-miR-2392 FASTmer inhibitor design and construction***

The FAST (Facile Accelerated Specific Therapeutics) platform was used to design FASTmer inhibitors, which are composed of a nanobiohyrd molecule based on antisense peptide nucleic acid (PNA) moiety conjugated to nanoparticle for improved delivery and membrane transport. The PNA moiety was chosen to be 15 bases long (in order to maximize both solubility and specificity), which yielded six potential target sequences within the 20-nucleotide mature human miR-2392. These potential targets were screened using FAST for solubility, self-complementing sequences, and off-targeting within the human genome (GCF\_000001405.26) and SARS-CoV-2 viral genome (NC\_045512). The antisense sequence complementing miR-2392 nucleotides 2 to 16 (TCTCACCCCATCCT) was chosen in order to minimize off-targeting while maximizing coverage of the miR-2392 seed region. The FASTmer was synthesized (with an N-terminal histidine tag and a 2-(2-(2-aminoethoxy)ethoxy)acetic acid linker) on an Apex 396 peptide synthesizer (AAPPTec, LLC) with solid-phase Fmoc chemistry. Fmoc-PNA monomers were obtained from PolyOrg Inc., with A, C, and G monomers protected with Bhoc groups. Following synthesis, the peptides were conjugated with nanoparticles and purified via size-exclusion filtration. Conjugation and concentration of the purified solution was monitored through measurement of absorbance at 260 nm (for detection of PNA) and 400 nm (for quantification of gold nanoparticles).

## **QUANTIFICATION AND STATISTICAL ANALYSIS**

### ***Analysis of BALF RNA-seq data***

Bam files were imported into Partek Genome Studio v7.0, and gene expression values quantified vs the Grch38 reference annotation guide (Ensembl v99). Samples with fewer than 2 million aligned reads were excluded from further analysis. Genes with fewer than 10 reads in 25% of samples were excluded, and differential gene expression determined using ANOVA with infection status as contrast. Differentially expressed gene files were used in GSEA and IPA to determine biological significance and pathways being regulated.

### ***Analysis of Nasopharyngeal Swab RNA-seq data***



The nasopharyngeal swab samples were analyzed comparing COVID-19 viral infection to the negative patients and was as previously described in Butler et al. (Butler et al., 2021) and the DESeq2 (Love et al., 2014) was utilized to generate the differential expression data. Heatmaps were displayed using pheatmap (Kolde, 2015). Volcano plots were made use R program EnhancedVolcano (Blighe et al., 2018).

### ***Analysis of Autopsy RNA-seq data***

The full methods of the analysis from the autopsy patients is currently available in the Park et al. (Park et al., 2021). Briefly, RNA-seq data was processed through the nf-core/rnaseq pipeline (Ewels et al., 2020). This workflow involved adapter trimming using Trim Galore! (<https://github.com/FelixKrueger/TrimGalore>), read alignment with STAR (Dobin et al., 2013), gene quantification with Salmon (Patro et al., 2017), duplicate read marking with Picard MarkDuplicates (<https://github.com/broadinstitute/picard>), and transcript quantification with StringTie (Kovaka et al., 2019). Other quality control measures included RSeQC, Qualimap, and dupRadar. Alignment was performed using the GRCh38 build native to nf-core and annotation was performed using Gencode Human Release 33 (GRCH38.p13). FeatureCounts reads were normalized using variance-stabilizing transform (vst) in DESeq2 package in R for visualization purposes in log-scale (Love et al., 2014). Differential expression of genes were calculated by DESeq2. Differential expression comparisons were done as either COVID+ cases versus COVID- controls for each tissue specifically, correcting for sequencing batches with a covariate where applicable, or pairwise comparison of viral levels from the lung as determined by nCounter data. Volcano plots were made use R program EnhancedVolcano (Blighe et al., 2018).

### ***Analysis Combining Autopsy and Nasopharyngeal Swab RNA-seq data***

To combine the results from the autopsy and nasopharyngeal swab RNA-seq data, we utilized the t-score values from the DESeq2 analysis. Heatmaps were displayed using pheatmap (Kolde, 2015).

### ***Gene Set Enrichment Analysis (GSEA)***

For pathway analysis on the miR-2392 targets (**Fig. 3**) we utilized ShinyGO (Ge et al., 2020) to determine the significantly regulated pathways for each main cluster in the heatmap. The clustering was determined through k-mean statistics.

For pathway analysis on the miR-2392 mimic RNA-seq data, we utilized fast Gene Set Enrichment Analysis (fGSEA) (Korotkevich et al., 2021). Pathway analysis was done comparing miR-2392 mimics to all controls and the ranked list of genes were defined by the t-score statistics. The statistical significance was determined by 1000 permutations of the genesets (Subramanian et al., 2005).

### ***Analysis of proteomic and transcriptomic blood datasets from COVID-19 patients***

For the analysis of the miR-2392 targets in the blood tissue, we downloaded whole blood transcriptome data and plasma proteome data from The COVIDome Explorer Researcher Portal (Sullivan et al., 2021). For Transcriptome data we used the following filters: Category "Effect of COVID-19 status", Platform "Blood", Statistical test "Student's t-test", Adjustment method

"none", Sex "male" and "female", Age Group "All". For Proteome data we used the following filters: Category "Effect of COVID-19 status", Platform "SOMAscan", Statistical test "Student's t-test", Adjustment method "none", Sex "male" and "female", Age Group "All". We created the list of the intersecting genes from both datasets. We analyzed the list using RStudio Desktop 1.3.1093 (RStudio Team (2020). RStudio: Integrated Development Environment for R. RStudio, PBC, Boston, MA URL <http://www.rstudio.com/>), and visualized data using ggplot2 version 3.3.2 (Wickham, 2016) and ggrepel version 0.8.2 (<https://ggrepel.slowkow.com/>).

### ***Analysis of Monocyte RNA-seq data***

The monocyte COVID-19 RNA-Seq data, published under the accession GSE159678 (Rother et al., 2020), was downloaded from SRA and gene expression was quantified using Salmon's selective alignment approach (Srivastava et al., 2020). The RNA-Seq processing pipeline was implemented using pyrpipe (Singh et al., 2021) ([https://github.com/urmi-21/pyrpipe/tree/master/case\\_studies/Covid\\_RNA-Seq](https://github.com/urmi-21/pyrpipe/tree/master/case_studies/Covid_RNA-Seq)). Exploratory data analysis and differential expression analysis were performed using MetaOmGraph (Singh et al., 2020).

### ***Analysis of A549, Calu-3, NHBE, and COVID lung biopsy data***

Each data series was normalized and filtered for low-expressed genes (counts<1). Cell culture samples treated with SARS-CoV-2 were compared to untreated controls and COVID-19-positive patient samples were compared to healthy lung biopsies. Differentially expressed genes were determined from the R-program Limma-Voom (Ritchie et al., 2015) using a linear model with weighted least squares for each gene and the false discovery rate adjusted p-values were calculated.

### ***Analysis of miR-2392 mimic RNA-seq data***

Differential gene expression was determined using LIMMA-voom (Ritchie et al., 2015). Data were filtered to ensure data contained at least 5 million aligned reads, and average gene counts of > 10. Cell treatments we used as contrasts for differentially expressed gene calculations. These results were then uploaded to GSEA for further analysis. (R script in supplementary section)

### ***Conservation of miR-2392 between species***

To determine conservation of miR-2392 among different species we utilized UCSC Genome Browser (Kent et al., 2002). Hsa-miR-2392 was entered as an input and a select of species was used to compare which included common species that are currently used in SARS-CoV-2 *in vivo* studies (i.e. mice, ferrets, and hamsters). We also chose primates and other animals to provide a wide spectrum of species to observe conservation of miR-2392. Lastly, the UCSC Genome Browser provides the host gene for miR-2392 (i.e. MEG3) and redirects to GTEx (Consortium, 2020) to provide a plot of MEG3 levels based on RNA-seq data on normal tissues.

### ***Mapping miR-2392 sequence to SARS-CoV-2 sequences***

To explore potential binding sites for miR-2392 we used miRanda software (Enright et al., 2003) to identify all potential binding sites with respect to the SARS-CoV-2 reference genome

(Wuhan-Hu-1; NC045512.2) and representative genomes from lineages of concern. The lineages of concern were selected from Global Initiative on Sharing All Influenza Data (GISAID) with each lineage being represented by 14 recent genomes.

### ***In silico predictions of genes from miRNAs***

Through the use of a Cytoscape (Shannon et al., 2003) plug-in called ClueGo/CluePedia (Bindea et al., 2013), we were able to predict genes targeted by the miRNAs determined. This involved entering all miRNAs in ClueGo and allowing the software to determine the top 50 genes that were significantly regulated and connected to the miRNAs. The predictions only reflect the functions that will be regulated by the miRNAs and do not show whether the function will be activated or inhibited. Lastly, miRNet 2.0 was utilized to predict the diseases and pathways that are associated with the miRNAs (Chang et al., 2020a). This was plotted as a dot utilizing the R-program ggplot2 (v3.2.1) (Wickham, 2016).

### ***ddPCR analysis of miRNA levels in patient samples***

First, we normalized the amount of each miRNA measured per body location (nasal, serum, and urine) using the general logarithm transformation. We compared miRNA levels in samples from patients either positive or negative for SARS-nCoV-2 using the student's t-test (unadjusted) as well as controlling for sex and age using least squares adjustment. Next, we generated receiver operating characteristic curves from each body location to show the performance of a classification model (SARS-nCoV-2 positive versus negative) at all classification thresholds using the absolute, non-transformed levels (miRNA copies per 5 ng RNA). Finally, we performed a subanalysis on each location to compare the variance of each miRNA in SARS-nCoV-2 negative patients compared to other patient groups. For serum and nasal samples, 1-way ANOVA was used to identify variation associated with the patient classification. For urine samples, 2-way ANOVA was used with location (outpatient versus inpatient) and SARS-nCoV-2 positivity as the main factors. If the ANOVA yielded a  $P < 0.05$ , Dunnett's post-test was used to compare subgroup means to the negative patient sample mean.

### ***Computational drug repositioning model***

Using the SM2miR database (Liu et al., 2013), we assembled an  $n \times m$  binary matrix ( $X$ ) containing 3,593 associations between small molecules ( $n = 213$ , rows) and miRNAs ( $m = 1,519$ , columns). Each matrix entry ( $X_{ij}$ ) was assigned a value of 1 where a small molecule is known to be associated to miRNA, and was 0 otherwise. The chemical notation as a simplified molecular input line entry system (SMILES) was obtained for each small molecule from PubChem. We then calculated the 2D Tanimoto chemical similarity between pairs of small molecules using the MACCS key binary fingerprints with RDKit (RDKit: Open-source cheminformatics; <http://www.rdkit.org>). Similarly, for each miRNA, we obtained its sequence from miRbase (Kozomara et al., 2019) and computed sequence similarity between miRNAs as the score of their Needleman-Wunsch alignment. We used the binary matrix, together with the chemical and sequence similarities, as input to our state-of-the-art drug target prediction model to predict missing associations in  $X$  (Galeano et al., 2021). The model parameters where:  $p = \frac{1}{2}$ ,

$\beta_{\text{Chem}} = 1$ , and  $\alpha_{\text{seq}} = 0$ . To assess the prediction performance of the model, we performed ten-fold cross-validation simulations.

## References

- Allegra, L., Dal Sasso, M., Bovio, C., Massoni, C., Fonti, E., and Braga, P.C. (2002). Human neutrophil oxidative bursts and their in vitro modulation by different N-acetylcysteine concentrations. *Arzneimittelforschung* 52, 669-676.
- Ardestani, A., and Azizi, Z. (2021). Targeting glucose metabolism for treatment of COVID-19. *Signal Transduct Target Ther* 6, 112.
- Asai, A., Konno, M., Ozaki, M., Otsuka, C., Vecchione, A., Arai, T., Kitagawa, T., Ofusa, K., Yabumoto, M., Hirotsu, T., *et al.* (2020). COVID-19 Drug Discovery Using Intensive Approaches. *Int J Mol Sci* 21.
- Aunins, T.R., Erickson, K.E., and Chatterjee, A. (2020). Transcriptome-based design of antisense inhibitors potentiates carbapenem efficacy in CRE *Escherichia coli*. *Proc Natl Acad Sci U S A* 117, 30699-30709.
- Aykin-Burns, N., Franklin, E.A., and Ercal, N. (2005). Effects of N-acetylcysteine on lead-exposed PC-12 cells. *Arch Environ Contam Toxicol* 49, 119-123.
- Baden, L.R., El Sahly, H.M., Essink, B., Kotloff, K., Frey, S., Novak, R., Diemert, D., Spector, S.A., Rouphael, N., Creech, C.B., *et al.* (2021). Efficacy and Safety of the mRNA-1273 SARS-CoV-2 Vaccine. *N Engl J Med* 384, 403-416.
- Bartoszewski, R., Dabrowski, M., Jakiela, B., Matalon, S., Harrod, K.S., Sanak, M., and Collawn, J.F. (2020). SARS-CoV-2 may regulate cellular responses through depletion of specific host miRNAs. *Am J Physiol Lung Cell Mol Physiol* 319, L444-L455.
- Bindea, G., Galon, J., and Mlecnik, B. (2013). CluePedia Cytoscape plugin: pathway insights using integrated experimental and in silico data. *Bioinformatics* 29, 661-663.
- Bindea, G., Mlecnik, B., Hackl, H., Charoentong, P., Tosolini, M., Kirilovsky, A., Fridman, W.H., Pages, F., Trajanoski, Z., and Galon, J. (2009). ClueGO: a Cytoscape plug-in to decipher functionally grouped gene ontology and pathway annotation networks. *Bioinformatics* 25, 1091-1093.
- Blanco-Melo, D., Nilsson-Payant, B.E., Liu, W.C., Uhl, S., Hoagland, D., Moller, R., Jordan, T.X., Oishi, K., Panis, M., Sachs, D., *et al.* (2020). Imbalanced Host Response to SARS-CoV-2 Drives Development of COVID-19. *Cell* 181, 1036-1045 e1039.
- Blighe, K., Rana, S., and Lewis, M. (2018). EnhancedVolcano: Publication-ready volcano plots with enhanced colouring and labeling. <https://github.com/kevinblighe/EnhancedVolcano>.
- Butler, D., Mozsary, C., Meydan, C., Foux, J., Rosiene, J., Shaiber, A., Danko, D., Afshinnkoo, E., MacKay, M., Sedlazeck, F.J., *et al.* (2021). Shotgun transcriptome, spatial omics, and isothermal profiling of SARS-CoV-2 infection reveals unique host responses, viral diversification, and drug interactions. *Nat Commun* 12, 1660.
- Carboni, E., Carta, A.R., and Carboni, E. (2020). Can pioglitazone be potentially useful therapeutically in treating patients with COVID-19? *Med Hypotheses* 140, 109776.



1328 Carfi, A., Bernabei, R., Landi, F., and Gemelli Against, C.-P.-A.C.S.G. (2020). Persistent  
1329 Symptoms in Patients After Acute COVID-19. *JAMA* 324, 603-605.

1330 Carrico, C., Meyer, J.G., He, W., Gibson, B.W., and Verdin, E. (2018). The Mitochondrial  
1331 Acylome Emerges: Proteomics, Regulation by Sirtuins, and Metabolic and Disease Implications.  
1332 *Cell Metab* 27, 497-512.

1333 Centa, A., Fonseca, A.S., Ferreira, S., Azevedo, M.L.V., Vaz de Paula, C.B., Nagashima, S.,  
1334 Machado-Souza, C., Miggiolaro, A., Baena, C.P., de Noronha, L., *et al.* (2020). Deregulated  
1335 miRNA expression is associated with endothelial dysfunction in post-mortem lung biopsies of  
1336 COVID-19 patients. *Am J Physiol Lung Cell Mol Physiol*.

1337 Chang, L., Zhou, G., Soufan, O., and Xia, J. (2020a). miRNet 2.0: network-based visual  
1338 analytics for miRNA functional analysis and systems biology. *Nucleic Acids Res*.

1339 Chang, L., Zhou, G., Soufan, O., and Xia, J. (2020b). miRNet 2.0: network-based visual  
1340 analytics for miRNA functional analysis and systems biology. *Nucleic Acids Res* 48, W244-  
1341 W251.

1342 Chen, J., Yao, D., Li, Y., Chen, H., He, C., Ding, N., Lu, Y., Ou, T., Zhao, S., Li, L., *et al.*  
1343 (2013). Serum microRNA expression levels can predict lymph node metastasis in patients with  
1344 early-stage cervical squamous cell carcinoma. *Int J Mol Med* 32, 557-567.

1345 Chen, Y., and Wang, X. (2020). miRDB: an online database for prediction of functional  
1346 microRNA targets. *Nucleic Acids Res* 48, D127-D131.

1347 Condorelli, G., Latronico, M.V., and Dorn, G.W., 2nd (2010). microRNAs in heart disease:  
1348 putative novel therapeutic targets? *Eur Heart J* 31, 649-658.

1349 Consortium, G.T. (2020). The GTEx Consortium atlas of genetic regulatory effects across human  
1350 tissues. *Science* 369, 1318-1330.

1351 Dickey, L.L., Worne, C.L., Glover, J.L., Lane, T.E., and O'Connell, R.M. (2016). MicroRNA-  
1352 155 enhances T cell trafficking and antiviral effector function in a model of coronavirus-induced  
1353 neurologic disease. *J Neuroinflammation* 13, 240.

1354 Dobin, A., Davis, C.A., Schlesinger, F., Drenkow, J., Zaleski, C., Jha, S., Batut, P., Chaisson,  
1355 M., and Gingeras, T.R. (2013). STAR: ultrafast universal RNA-seq aligner. *Bioinformatics* 29,  
1356 15-21.

1357 Dweep, H., and Gretz, N. (2015). miRWalk2.0: a comprehensive atlas of microRNA-target  
1358 interactions. *Nat Methods* 12, 697.

1359 Edmonds, C.E., Zuckerman, S.P., and Conant, E.F. (2021). Management of Unilateral Axillary  
1360 Lymphadenopathy Detected on Breast MRI in the Era of Coronavirus Disease (COVID-19)  
1361 Vaccination. *AJR Am J Roentgenol*.

1362 Eller, K.A., Aunins, T.R., Courtney, C.M., Campos, J.K., Otoupal, P.B., Erickson, K.E.,  
1363 Madinger, N.E., and Chatterjee, A. (2021). Facile accelerated specific therapeutic (FAST)  
1364 platform develops antisense therapies to counter multidrug-resistant bacteria. *Commun Biol* 4,  
1365 331.

1366 Enomoto, Y., Takagi, R., Naito, Y., Kuniwa, T., Tanaka, Y., Hamada-Tsutsumi, S., Kawano, M.,  
1367 Matsushita, S., Ochiya, T., and Miyajima, A. (2017). Identification of the novel 3' UTR  
1368 sequences of human IL-21 mRNA as potential targets of miRNAs. *Sci Rep* 7, 7780.

1369 Enright, A.J., John, B., Gaul, U., Tuschl, T., Sander, C., and Marks, D.S. (2003). MicroRNA  
1370 targets in *Drosophila*. *Genome Biol* 5, R1.

1371 Ewels, P.A., Peltzer, A., Fillinger, S., Patel, H., Alneberg, J., Wilm, A., Garcia, M.U., Di  
1372 Tommaso, P., and Nahnsen, S. (2020). The nf-core framework for community-curated  
1373 bioinformatics pipelines. *Nat Biotechnol* 38, 276-278.

1374 Fan, S., Tian, T., Chen, W., Lv, X., Lei, X., Zhang, H., Sun, S., Cai, L., Pan, G., He, L., *et al.*  
1375 (2019). Mitochondrial miRNA Determines Chemoresistance by Reprogramming Metabolism  
1376 and Regulating Mitochondrial Transcription. *Cancer research* 79, 1069-1084.

1377 Feng, L., Yin, Y.Y., Liu, C.H., Xu, K.R., Li, Q.R., Wu, J.R., and Zeng, R. (2020). Proteome-  
1378 wide Data Analysis Reveals Tissue-specific Network Associated with SARS-CoV-2 Infection. *J*  
1379 *Mol Cell Biol*.

1380 Friedman, R.C., Farh, K.K., Burge, C.B., and Bartel, D.P. (2009). Most mammalian mRNAs are  
1381 conserved targets of microRNAs. *Genome Res* 19, 92-105.

1382 Galeano, D., Noto, S., Jimenez, R., and Paccanaro, A. (2021). Interpretable Drug Target  
1383 Predictions using Self-Expressiveness. *bioRxiv*, 2021.2003.2001.433365.

1384 Ge, S.X., Jung, D., and Yao, R. (2020). ShinyGO: a graphical gene-set enrichment tool for  
1385 animals and plants. *Bioinformatics* 36, 2628-2629.

1386 Gharebaghi, R., Heidary, F., Moradi, M., and Parvizi, M. (2020). Metronidazole; a Potential  
1387 Novel Addition to the COVID-19 Treatment Regimen. *Arch Acad Emerg Med* 8, e40.

1388 Griffin, R.J., Monzen, H., Williams, B.W., Park, H., Lee, S.H., and Song, C.W. (2003). Arsenic  
1389 trioxide induces selective tumour vascular damage via oxidative stress and increases  
1390 thermosensitivity of tumours. *Int J Hyperthermia* 19, 575-589.

1391 Gudbjartsson, D.F., Norddahl, G.L., Melsted, P., Gunnarsdottir, K., Holm, H., Eythorsson, E.,  
1392 Arnthorsson, A.O., Helgason, D., Bjarnadottir, K., Ingvarsson, R.F., *et al.* (2020). Humoral  
1393 Immune Response to SARS-CoV-2 in Iceland. *N Engl J Med* 383, 1724-1734.

1394 Gupta, A., Madhavan, M.V., Sehgal, K., Nair, N., Mahajan, S., Sehrawat, T.S., Bikdeli, B.,  
1395 Ahluwalia, N., Ausiello, J.C., Wan, E.Y., *et al.* (2020). Extrapulmonary manifestations of  
1396 COVID-19. *Nat Med* 26, 1017-1032.

1397 Hemmat, N., Asadzadeh, Z., Ahangar, N.K., Alemohammad, H., Najafzadeh, B., Derakhshani,  
1398 A., Baghbanzadeh, A., Baghi, H.B., Javadrashid, D., Najafi, S., *et al.* (2021). The roles of  
1399 signaling pathways in SARS-CoV-2 infection; lessons learned from SARS-CoV and MERS-  
1400 CoV. *Archives of Virology* 166, 675-696.

1401 Herrmann, J., Mori, V., Bates, J.H.T., and Suki, B. (2020). Modeling lung perfusion  
1402 abnormalities to explain early COVID-19 hypoxemia. *Nat Commun* 11, 4883.

1403 Ho, W.Z., and Douglas, S.D. (1992). Glutathione and N-acetylcysteine suppression of human  
1404 immunodeficiency virus replication in human monocyte/macrophages in vitro. *AIDS Res Hum*  
1405 *Retroviruses* 8, 1249-1253.

1406 Hou, X., Liang, Y., Chen, J., Wei, Y., Zeng, P., Wang, L., Lu, C., and Diao, H. (2017).  
1407 Expression Profiling of Cellular MicroRNA in Asymptomatic HBsAg Carriers and Chronic  
1408 Hepatitis B Patients. *Biomed Res Int* 2017, 6484835.

1409 Hou, Z., Fan, F., and Liu, P. (2019). BTXA regulates the epithelial-mesenchymal transition and  
1410 autophagy of keloid fibroblasts via modulating miR-1587/miR-2392 targeted ZEB2. *Biosci Rep*  
1411 39.

1412 Hu, H.M., Chen, Y., Liu, L., Zhang, C.G., Wang, W., Gong, K., Huang, Z., Guo, M.X., Li,  
1413 W.X., and Li, W. (2013). C1orf61 acts as a tumor activator in human hepatocellular carcinoma  
1414 and is associated with tumorigenesis and metastasis. *FASEB J* 27, 163-173.

1415 Hu, S., Li, Z., Lan, Y., Guan, J., Zhao, K., Chu, D., Fan, G., Guo, Y., Gao, F., and He, W.  
1416 (2020). MiR-10a-5p-Mediated Syndecan 1 Suppression Restricts Porcine Hemagglutinating  
1417 Encephalomyelitis Virus Replication. *Front Microbiol* 11, 105.

1418 Huang, C., Wang, Y., Li, X., Ren, L., Zhao, J., Hu, Y., Zhang, L., Fan, G., Xu, J., Gu, X., *et al.*  
1419 (2020). Clinical features of patients infected with 2019 novel coronavirus in Wuhan, China.  
1420 *Lancet* 395, 497-506.

1421 Hultstrom, M., Lipcsey, M., Wallin, E., Larsson, I.M., Larsson, A., and Frithiof, R. (2021).  
1422 Severe acute kidney injury associated with progression of chronic kidney disease after critical  
1423 COVID-19. *Crit Care* 25, 37.

1424 Ibrahim, H., Perl, A., Smith, D., Lewis, T., Kon, Z., Goldenberg, R., Yarta, K., Staniloae, C., and  
1425 Williams, M. (2020). Therapeutic blockade of inflammation in severe COVID-19 infection with  
1426 intravenous N-acetylcysteine. *Clin Immunol* 219, 108544.

1427 Islam, M.S., and Islam, A.B.M.M.K. (2021). Viral miRNAs confer survival in host cells by  
1428 targeting apoptosis related host genes. *Informatics in Medicine Unlocked* 22, 100501.

1429 Jacobs, L.G., Gourni Paleoudis, E., Lesky-Di Bari, D., Nyirenda, T., Friedman, T., Gupta, A.,  
1430 Rasouli, L., Zetkovic, M., Balani, B., Ogedegbe, C., *et al.* (2020). Persistence of symptoms and  
1431 quality of life at 35 days after hospitalization for COVID-19 infection. *PLoS One* 15, e0243882.

1432 Janssen, H.L., Reesink, H.W., Lawitz, E.J., Zeuzem, S., Rodriguez-Torres, M., Patel, K., van der  
1433 Meer, A.J., Patock, A.K., Chen, A., Zhou, Y., *et al.* (2013). Treatment of HCV infection by  
1434 targeting microRNA. *N Engl J Med* 368, 1685-1694.

1435 Jia, D., Koonce, N.A., Griffin, R.J., Jackson, C., and Corry, P.M. (2010). Prevention and  
1436 mitigation of acute death of mice after abdominal irradiation by the antioxidant N-acetyl-cysteine  
1437 (NAC). *Radiat Res* 173, 579-589.

1438 Jiang, Q., Wang, Y., Hao, Y., Juan, L., Teng, M., Zhang, X., Li, M., Wang, G., and Liu, Y.  
1439 (2009). miR2Disease: a manually curated database for microRNA deregulation in human  
1440 disease. *Nucleic Acids Res* 37, D98-104.

1441 Jima, D.D., Zhang, J., Jacobs, C., Richards, K.L., Dunphy, C.H., Choi, W.W., Au, W.Y.,  
1442 Srivastava, G., Czader, M.B., Rizzieri, D.A., *et al.* (2010). Deep sequencing of the small RNA  
1443 transcriptome of normal and malignant human B cells identifies hundreds of novel microRNAs.  
1444 *Blood* 116, e118-127.

1445 Johansen, M.D., Irving, A., Montagutelli, X., Tate, M.D., Rudloff, I., Nold, M.F., Hansbro, N.G.,  
1446 Kim, R.Y., Donovan, C., Liu, G., *et al.* (2020). Animal and translational models of SARS-CoV-2  
1447 infection and COVID-19. *Mucosal Immunol* 13, 877-891.

1448 Jopling, C.L., Yi, M., Lancaster, A.M., Lemon, S.M., and Sarnow, P. (2005). Modulation of  
1449 hepatitis C virus RNA abundance by a liver-specific MicroRNA. *Science* 309, 1577-1581.

1450 Kent, W.J., Sugnet, C.W., Furey, T.S., Roskin, K.M., Pringle, T.H., Zahler, A.M., and Haussler,  
1451 D. (2002). The human genome browser at UCSC. *Genome Res* 12, 996-1006.

1452 Kharazmi, A., Nielsen, H., and Schiotz, P.O. (1988). N-acetylcysteine inhibits human neutrophil  
1453 and monocyte chemotaxis and oxidative metabolism. *Int J Immunopharmacol* 10, 39-46.

1454 Kolde, R. (2015). pheatmap: Pretty heatmaps [Software].

1455 Korotkevich, G., Sukhov, V., Budin, N., Shpak, B., Artyomov, M.N., and Sergushichev, A.  
1456 (2021). Fast gene set enrichment analysis. *bioRxiv*, 060012.

1457 Koumpa, F.S., Forde, C.T., and Manjaly, J.G. (2020). Sudden irreversible hearing loss post  
1458 COVID-19. *BMJ Case Rep* 13.

1459 Kovaka, S., Zimin, A.V., Pertea, G.M., Razaghi, R., Salzberg, S.L., and Pertea, M. (2019).  
1460 Transcriptome assembly from long-read RNA-seq alignments with StringTie2. *Genome Biol* 20,  
1461 278.

1462 Kozomara, A., Birgaoanu, M., and Griffiths-Jones, S. (2019). miRBase: from microRNA  
1463 sequences to function. *Nucleic Acids Res* 47, D155-D162.

1464 Krajewski, P.K., Maj, J., and Szepietowski, J.C. (2021). Cutaneous Hyperaesthesia in SARS-  
1465 CoV-2 Infection: Rare but not Unique Clinical Manifestation. *Acta Derm Venereol* 101,  
1466 adv00366.

1467 Lamb, J., Crawford, E.D., Peck, D., Modell, J.W., Blat, I.C., Wrobel, M.J., Lerner, J., Brunet,  
1468 J.P., Subramanian, A., Ross, K.N., *et al.* (2006). The Connectivity Map: using gene-expression  
1469 signatures to connect small molecules, genes, and disease. *Science* 313, 1929-1935.

1470 Lawrie, C.H., Gal, S., Dunlop, H.M., Pushkaran, B., Liggins, A.P., Pulford, K., Banham, A.H.,  
1471 Pezzella, F., Boulwood, J., Wainscoat, J.S., *et al.* (2008). Detection of elevated levels of tumour-  
1472 associated microRNAs in serum of patients with diffuse large B-cell lymphoma. *Br J Haematol*  
1473 141, 672-675.

1474 Ledford, H. (2020). Coronavirus breakthrough: dexamethasone is first drug shown to save lives.  
1475 *Nature* 582, 469.

1476 Li, J., Li, T., Lu, Y., Shen, G., Guo, H., Wu, J., Lei, C., Du, F., Zhou, F., Zhao, X., *et al.* (2017).  
1477 MiR-2392 suppresses metastasis and epithelial-mesenchymal transition by targeting MAML3  
1478 and WHSC1 in gastric cancer. *FASEB J* 31, 3774-3786.

1479 Li, K., Chen, G., Hou, H., Liao, Q., Chen, J., Bai, H., Lee, S., Wang, C., Li, H., Cheng, L., *et al.*  
1480 (2021). Analysis of sex hormones and menstruation in COVID-19 women of child-bearing age.  
1481 *Reprod Biomed Online* 42, 260-267.

1482 Liu, X., Wang, S., Meng, F., Wang, J., Zhang, Y., Dai, E., Yu, X., Li, X., and Jiang, W. (2013).  
1483 SM2miR: a database of the experimentally validated small molecules' effects on microRNA  
1484 expression. *Bioinformatics* 29, 409-411.

1485 Lott, M.T., Leipzig, J.N., Derbeneva, O., Xie, H.M., Chalkia, D., Sarmady, M., Procaccio, V.,  
1486 and Wallace, D.C. (2013). mtDNA Variation and Analysis Using Mitomap and Mitomaster. *Curr*  
1487 *Protoc Bioinformatics* 44, 1 23 21-26.

1488 Love, M.I., Huber, W., and Anders, S. (2014). Moderated estimation of fold change and  
1489 dispersion for RNA-seq data with DESeq2. *Genome Biol* 15, 550.



Loza, M.J., McCall, C.E., Li, L., Isaacs, W.B., Xu, J., and Chang, B.L. (2007). Assembly of inflammation-related genes for pathway-focused genetic analysis. *PLoS One* 2, e1035.

Ma, Y., Wang, C., Xue, M., Fu, F., Zhang, X., Li, L., Yin, L., Xu, W., Feng, L., and Liu, P. (2018). The Coronavirus Transmissible Gastroenteritis Virus Evades the Type I Interferon Response through IRE1alpha-Mediated Manipulation of the MicroRNA miR-30a-5p/SOCS1/3 Axis. *J Virol* 92.

Mahajan, A., and Mason, G.F. (2021). A sobering addition to the literature on COVID-19 and the brain. *J Clin Invest*.

Malik, Z.R., Razaq, Z., Siff, M., and Sheikh, S. (2020). COVID-19 Presenting as Banti's Syndrome. *Cureus* 12, e9096.

Mishra, P.K., Tandon, R., and Byrareddy, S.N. (2020). Diabetes and COVID-19 risk: an miRNA perspective. *Am J Physiol Heart Circ Physiol* 319, H604-H609.

Mitchell, P.S., Parkin, R.K., Kroh, E.M., Fritz, B.R., Wyman, S.K., Pogosova-Agadjanyan, E.L., Peterson, A., Noteboom, J., O'Briant, K.C., Allen, A., *et al.* (2008). Circulating microRNAs as stable blood-based markers for cancer detection. *Proc Natl Acad Sci U S A* 105, 10513-10518.

Nagy, A., Lanczky, A., Menyhart, O., and Gyorffy, B. (2018). Validation of miRNA prognostic power in hepatocellular carcinoma using expression data of independent datasets. *Sci Rep* 8, 9227.

Nagy, A., Munkacsy, G., and Gyorffy, B. (2021). Pancancer survival analysis of cancer hallmark genes. *Sci Rep* 11, 6047.

Nersisyan, S., Engibaryan, N., Gorbonos, A., Kirdey, K., Makhonin, A., and Tonevitsky, A. (2020). Potential role of cellular miRNAs in coronavirus-host interplay. *PeerJ* 8, e9994.

Nishiga, M., Wang, D.W., Han, Y., Lewis, D.B., and Wu, J.C. (2020). COVID-19 and cardiovascular disease: from basic mechanisms to clinical perspectives. *Nat Rev Cardiol* 17, 543-558.

Ochsner, S.A., Pillich, R.T., and McKenna, N.J. (2020). Consensus transcriptional regulatory networks of coronavirus-infected human cells. *Sci Data* 7, 314.

Ottosen, S., Parsley, T.B., Yang, L., Zeh, K., van Doorn, L.J., van der Veer, E., Raney, A.K., Hodges, M.R., and Patick, A.K. (2015). In vitro antiviral activity and preclinical and clinical resistance profile of miravirsin, a novel anti-hepatitis C virus therapeutic targeting the human factor miR-122. *Antimicrob Agents Chemother* 59, 599-608.

Park, J., Foon, J., Hether, T., Danko, D., Warren, S., Kim, Y., Reeves, J., Butler, D.J., Mozsary, C., Rosiene, J., *et al.* (2021). Systemic Tissue and Cellular Disruption from SARS-CoV-2 Infection revealed in COVID-19 Autopsies and Spatial Omics Tissue Maps. *bioRxiv*, 2021.2003.2008.434433.

Park, J.L., Park, S.M., Kwon, O.H., Lee, H.C., Kim, J.Y., Seok, H.H., Lee, W.S., Lee, S.H., Kim, Y.S., Woo, K.M., *et al.* (2014). Microarray screening and qRT-PCR evaluation of microRNA markers for forensic body fluid identification. *Electrophoresis* 35, 3062-3068.

Patro, R., Duggal, G., Love, M.I., Irizarry, R.A., and Kingsford, C. (2017). Salmon provides fast and bias-aware quantification of transcript expression. *Nat Methods* 14, 417-419.

1530 Polack, F.P., Thomas, S.J., Kitchin, N., Absalon, J., Gurtman, A., Lockhart, S., Perez, J.L., Perez  
1531 Marc, G., Moreira, E.D., Zerbini, C., *et al.* (2020). Safety and Efficacy of the BNT162b2 mRNA  
1532 Covid-19 Vaccine. *N Engl J Med* 383, 2603-2615.

1533 Pontecorvi, G., Bellenghi, M., Ortona, E., and Care, A. (2020). microRNAs as new possible  
1534 actors in gender disparities of Covid-19 pandemic. *Acta Physiol (Oxf)* 230, e13538.

1535 Poppe, M., Wittig, S., Jurida, L., Bartkuhn, M., Wilhelm, J., Muller, H., Beuerlein, K., Karl, N.,  
1536 Bhuj, S., Ziebuhr, J., *et al.* (2017). The NF-kappaB-dependent and -independent transcriptome  
1537 and chromatin landscapes of human coronavirus 229E-infected cells. *PLoS Pathog* 13,  
1538 e1006286.

1539 Portincasa, P., Krawczyk, M., Machill, A., Lammert, F., and Di Ciaula, A. (2020). Hepatic  
1540 consequences of COVID-19 infection. Lapping or biting? *Eur J Intern Med* 77, 18-24.

1541 Rath, S., Sharma, R., Gupta, R., Ast, T., Chan, C., Durham, T.J., Goodman, R.P., Grabarek, Z.,  
1542 Haas, M.E., Hung, W.H.W., *et al.* (2021). MitoCarta3.0: an updated mitochondrial proteome  
1543 now with sub-organellar localization and pathway annotations. *Nucleic Acids Res* 49, D1541-  
1544 D1547.

1545 Rodriguez, M., Soler, Y., Perry, M., Reynolds, J.L., and El-Hage, N. (2020). Impact of Severe  
1546 Acute Respiratory Syndrome Coronavirus 2 (SARS-CoV-2) in the Nervous System: Implications  
1547 of COVID-19 in Neurodegeneration. *Front Neurol* 11, 583459.

1548 Rossi, R., Talarico, M., Coppi, F., and Boriani, G. (2020). Protective role of statins in COVID 19  
1549 patients: importance of pharmacokinetic characteristics rather than intensity of action. *Intern*  
1550 *Emerg Med* 15, 1573-1576.

1551 Rother, N., Yanginlar, C., Lindeboom, R.G.H., Bekkering, S., van Leent, M.M.T., Buijsers, B.,  
1552 Jonkman, I., de Graaf, M., Baltissen, M., Lamers, L.A., *et al.* (2020). Hydroxychloroquine  
1553 Inhibits the Trained Innate Immune Response to Interferons. *Cell Rep Med* 1, 100146.

1554 Rupaimoole, R., and Slack, F.J. (2017). MicroRNA therapeutics: towards a new era for the  
1555 management of cancer and other diseases. *Nat Rev Drug Discov* 16, 203-222.

1556 Sacar Demirci, M.D., and Adan, A. (2020). Computational analysis of microRNA-mediated  
1557 interactions in SARS-CoV-2 infection. *PeerJ* 8, e9369.

1558 Sadoff, J., Le Gars, M., Shukarev, G., Heerwegh, D., Truysers, C., de Groot, A.M., Stoop, J.,  
1559 Tete, S., Van Damme, W., Leroux-Roels, I., *et al.* (2021). Interim Results of a Phase 1-2a Trial  
1560 of Ad26.COV2.S Covid-19 Vaccine. *N Engl J Med*.

1561 Sadowska, A.M., Manuel-y-Keenoy, B., Vertongen, T., Schippers, G., Radomska-Lesniewska,  
1562 D., Heytens, E., and De Backer, W.A. (2006). Effect of N-acetylcysteine on neutrophil activation  
1563 markers in healthy volunteers: in vivo and in vitro study. *Pharmacol Res* 53, 216-225.

1564 Sardar, R., Satish, D., and Gupta, D. (2020). Identification of Novel SARS-CoV-2 Drug Targets  
1565 by Host MicroRNAs and Transcription Factors Co-regulatory Interaction Network Analysis.  
1566 *Front Genet* 11, 571274.

1567 Schult, P., Roth, H., Adams, R.L., Mas, C., Imbert, L., Orlik, C., Ruggieri, A., Pyle, A.M., and  
1568 Lohmann, V. (2018). microRNA-122 amplifies hepatitis C virus translation by shaping the  
1569 structure of the internal ribosomal entry site. *Nat Commun* 9, 2613.

Self, W.H., Tenforde, M.W., Stubblefield, W.B., Feldstein, L.R., Steingrub, J.S., Shapiro, N.I., Ginde, A.A., Prekker, M.E., Brown, S.M., Peltan, I.D., *et al.* (2020). Decline in SARS-CoV-2 Antibodies After Mild Infection Among Frontline Health Care Personnel in a Multistate Hospital Network - 12 States, April-August 2020. *MMWR Morb Mortal Wkly Rep* 69, 1762-1766.

Shannon, P., Markiel, A., Ozier, O., Baliga, N.S., Wang, J.T., Ramage, D., Amin, N., Schwikowski, B., and Ideker, T. (2003). Cytoscape: a software environment for integrated models of biomolecular interaction networks. *Genome Res* 13, 2498-2504.

Shu, Y., and McCauley, J. (2017). GISAID: Global initiative on sharing all influenza data - from vision to reality. *Euro Surveill* 22.

Singh, U., Hur, M., Dorman, K., and Wurtele, E.S. (2020). MetaOmGraph: a workbench for interactive exploratory data analysis of large expression datasets. *Nucleic Acids Res* 48, e23.

Singh, U., Li, J., Seetharam, A., and Wurtele, E.S. (2021). pyrpipeline: a python package for RNA-Seq workflows. *bioRxiv*, 2020.2003.2004.925818.

Sirin, D.A., and Ozcelik, F. (2021). The relationship between COVID-19 and the dental damage stage determined by radiological examination. *Oral Radiol*.

Sirota, M., Dudley, J.T., Kim, J., Chiang, A.P., Morgan, A.A., Sweet-Cordero, A., Sage, J., and Butte, A.J. (2011). Discovery and preclinical validation of drug indications using compendia of public gene expression data. *Sci Transl Med* 3, 96ra77.

Srivastava, A., Malik, L., Sarkar, H., Zakeri, M., Almodaresi, F., Soneson, C., Love, M.I., Kingsford, C., and Patro, R. (2020). Alignment and mapping methodology influence transcript abundance estimation. *Genome Biol* 21, 239.

Su, M., Chen, Y., Qi, S., Shi, D., Feng, L., and Sun, D. (2020). A Mini-Review on Cell Cycle Regulation of Coronavirus Infection. *Front Vet Sci* 7, 586826.

Subramanian, A., Tamayo, P., Mootha, V.K., Mukherjee, S., Ebert, B.L., Gillette, M.A., Paulovich, A., Pomeroy, S.L., Golub, T.R., Lander, E.S., *et al.* (2005). Gene set enrichment analysis: a knowledge-based approach for interpreting genome-wide expression profiles. *Proc Natl Acad Sci U S A* 102, 15545-15550.

Sullivan, K.D., Galbraith, M.D., Kinning, K.T., Bartsch, K., Levinsky, N., Araya, P., Smith, K.P., Granrath, R.E., Shaw, J.R., Baxter, R., *et al.* (2021). The COVIDome Explorer Researcher Portal. *medRxiv*.

Tang, H., Gao, Y., Li, Z., Miao, Y., Huang, Z., Liu, X., Xie, L., Li, H., Wen, W., Zheng, Y., *et al.* (2020). The noncoding and coding transcriptional landscape of the peripheral immune response in patients with COVID-19. *Clin Transl Med* 10, e200.

Teodori, L., Sestili, P., Madiati, V., Coppari, S., Fraternali, D., Rocchi, M.B.L., Ramakrishna, S., and Albertini, M.C. (2020). MicroRNAs Bioinformatics Analyses Identifying HDAC Pathway as a Putative Target for Existing Anti-COVID-19 Therapeutics. *Front Pharmacol* 11, 582003.

Thibault, P.A., Huys, A., Amador-Canizares, Y., Gailius, J.E., Pinel, D.E., and Wilson, J.A. (2015). Regulation of Hepatitis C Virus Genome Replication by Xrn1 and MicroRNA-122 Binding to Individual Sites in the 5' Untranslated Region. *J Virol* 89, 6294-6311.

1609 Tribolet, L., Kerr, E., Cowled, C., Bean, A.G.D., Stewart, C.R., Dearnley, M., and Farr, R.J.  
1610 (2020). MicroRNA Biomarkers for Infectious Diseases: From Basic Research to Biosensing.  
1611 *Front Microbiol* *11*, 1197.

1612 Trobaugh, D.W., and Klimstra, W.B. (2017). MicroRNA Regulation of RNA Virus Replication  
1613 and Pathogenesis. *Trends Mol Med* *23*, 80-93.

1614 V'Kovski, P., Kratzel, A., Steiner, S., Stalder, H., and Thiel, V. (2021). Coronavirus biology and  
1615 replication: implications for SARS-CoV-2. *Nat Rev Microbiol* *19*, 155-170.

1616 van der Ree, M.H., de Vree, J.M., Stelma, F., Willemse, S., van der Valk, M., Rietdijk, S.,  
1617 Molenkamp, R., Schinkel, J., van Nuenen, A.C., Beuers, U., *et al.* (2017). Safety, tolerability,  
1618 and antiviral effect of RG-101 in patients with chronic hepatitis C: a phase 1B, double-blind,  
1619 randomised controlled trial. *Lancet* *389*, 709-717.

1620 Vejnar, C.E., and Zdobnov, E.M. (2012). MiRmap: comprehensive prediction of microRNA  
1621 target repression strength. *Nucleic Acids Res* *40*, 11673-11683.

1622 Wallace, D.C. (2018). Mitochondrial genetic medicine. *Nat Genet* *50*, 1642-1649.

1623 Walsh-Messinger, J., Manis, H., Vrabec, A., Sizemore, J., Bishof, K., Debidia, M., Malaspina,  
1624 D., and Greenspan, N. (2020). The Kids Are Not Alright: A Preliminary Report of Post-COVID  
1625 Syndrome in University Students. *medRxiv*.

1626 West, A.P., Khoury-Hanold, W., Staron, M., Tal, M.C., Pineda, C.M., Lang, S.M., Bestwick, M.,  
1627 Duguay, B.A., Raimundo, N., MacDuff, D.A., *et al.* (2015). Mitochondrial DNA stress primes  
1628 the antiviral innate immune response. *Nature* *520*, 553-557.

1629 West, A.P., and Shadel, G.S. (2017). Mitochondrial DNA in innate immune responses and  
1630 inflammatory pathology. *Nat Rev Immunol* *17*, 363-375.

1631 Wickham, H. (2016). *ggplot2: Elegant Graphics for Data Analysis* (Springer-Verlag New York).

1632 Widiasta, A., Sribudiani, Y., Nugrahapraja, H., Hilmanto, D., Sekarwana, N., and Rachmadi, D.  
1633 (2020). Potential role of ACE2-related microRNAs in COVID-19-associated nephropathy.  
1634 *Noncoding RNA Res* *5*, 153-166.

1635 Yang, J., Li, C., Li, H., and E, C. (2019). LncRNA CACNA1G-AS1 facilitates hepatocellular  
1636 carcinoma progression through the miR-2392/C1orf61 pathway. *J Cell Physiol* *234*, 18415-  
1637 18422.

1638 Yang, S., Pei, Y., Li, X., Zhao, S., Zhu, M., and Zhao, A. (2016). miR-124 attenuates Japanese  
1639 encephalitis virus replication by targeting DNM2. *Virology* *13*, 105.

1640 Younis, J.S., Abassi, Z., and Skorecki, K. (2020). Is there an impact of the COVID-19 pandemic  
1641 on male fertility? The ACE2 connection. *Am J Physiol Endocrinol Metab* *318*, E878-E880.

1642 Zamani, B., Moeini Taba, S.M., and Shayestehpour, M. (2021). Systemic lupus erythematosus  
1643 manifestation following COVID-19: a case report. *J Med Case Rep* *15*, 29.

1644 Zhong, Z., Liang, S., Sanchez-Lopez, E., He, F., Shalapour, S., Lin, X.J., Wong, J., Ding, S.,  
1645 Seki, E., Schnabl, B., *et al.* (2018). New mitochondrial DNA synthesis enables NLRP3  
1646 inflammasome activation. *Nature* *560*, 198-203.

1647 Zhu, N., Zhang, D., Wang, W., Li, X., Yang, B., Song, J., Zhao, X., Huang, B., Shi, W., Lu, R.,  
1648 *et al.* (2020). A Novel Coronavirus from Patients with Pneumonia in China, 2019. *N Engl J Med*  
1649 *382*, 727-733.



1650 Abdelrahman, Z., Liu, Q., Jiang, S., Li, M., Sun, Q., Zhang, Y., and Wang, X. (2021). Evaluation  
1651 of the Current Therapeutic Approaches for COVID-19: A Systematic Review and a Meta-  
1652 analysis. *Front Pharmacol* 12, 607408.

1653 Alamdari, D.H., Moghaddam, A.B., Amini, S., Keramati, M.R., Zarmehri, A.M., Alamdari,  
1654 A.H., Damsaz, M., Banpour, H., Yarahmadi, A., and Koliakos, G. (2020). Application of  
1655 methylene blue -vitamin C -N-acetyl cysteine for treatment of critically ill COVID-19 patients,  
1656 report of a phase-I clinical trial. *Eur J Pharmacol* 885, 173494.

1657 Ardestani, A., and Azizi, Z. (2021). Targeting glucose metabolism for treatment of COVID-19.  
1658 *Signal Transduct Target Ther* 6, 112.

1659 Bojkova, D., Klann, K., Koch, B., Widera, M., Krause, D., Ciesek, S., Cinatl, J., and Munch, C.  
1660 (2020). Proteomics of SARS-CoV-2-infected host cells reveals therapy targets. *Nature* 583, 469-  
1661 472.

1662 Codo, A.C., Davanzo, G.G., Monteiro, L.B., de Souza, G.F., Muraro, S.P., Virgilio-da-Silva,  
1663 J.V., Prodonoff, J.S., Carregari, V.C., de Biagi Junior, C.A.O., Crunfli, F., *et al.* (2020). Elevated  
1664 Glucose Levels Favor SARS-CoV-2 Infection and Monocyte Response through a HIF-  
1665 1alpha/Glycolysis-Dependent Axis. *Cell Metab* 32, 437-446 e435.

1666 Mishra, P.K., Tandon, R., and Byrareddy, S.N. (2020). Diabetes and COVID-19 risk: an miRNA  
1667 perspective. *Am J Physiol Heart Circ Physiol* 319, H604-H609.

1668 Nersisyan, S., Engibaryan, N., Gorbonos, A., Kirdey, K., Makhonin, A., and Tonevitsky, A.  
1669 (2020). Potential role of cellular miRNAs in coronavirus-host interplay. *PeerJ* 8, e9994.

1670 Overbey, E.G., Saravia-Butler, A.M., Zhang, Z., Rathi, K.S., Fogle, H., da Silveira, W.A.,  
1671 Barker, R.J., Bass, J.J., Beheshti, A., Berrios, D.C., *et al.* (2021). NASA GeneLab RNA-seq  
1672 consensus pipeline: standardized processing of short-read RNA-seq data. *iScience* 24.

1673 Portincasa, P., Krawczyk, M., Machill, A., Lammert, F., and Di Ciaula, A. (2020). Hepatic  
1674 consequences of COVID-19 infection. Lapping or biting? *Eur J Intern Med* 77, 18-24.

1675 Ren, L., Zhang, R., Rao, J., Xiao, Y., Zhang, Z., Yang, B., Cao, D., Zhong, H., Ning, P., Shang,  
1676 Y., *et al.* (2018). Transcriptionally Active Lung Microbiome and Its Association with Bacterial  
1677 Biomass and Host Inflammatory Status. *mSystems* 3.

1678 Ritchie, M.E., Phipson, B., Wu, D., Hu, Y., Law, C.W., Shi, W., and Smyth, G.K. (2015). limma  
1679 powers differential expression analyses for RNA-sequencing and microarray studies. *Nucleic  
1680 Acids Res* 43, e47.

1681 Sacar Demirci, M.D., and Adan, A. (2020). Computational analysis of microRNA-mediated  
1682 interactions in SARS-CoV-2 infection. *PeerJ* 8, e9369.

1683 Sardar, R., Satish, D., and Gupta, D. (2020). Identification of Novel SARS-CoV-2 Drug Targets  
1684 by Host MicroRNAs and Transcription Factors Co-regulatory Interaction Network Analysis.  
1685 *Front Genet* 11, 571274.

1686 Shen, Z., Xiao, Y., Kang, L., Ma, W., Shi, L., Zhang, L., Zhou, Z., Yang, J., Zhong, J., Yang, D.,  
1687 *et al.* (2020). Genomic Diversity of Severe Acute Respiratory Syndrome-Coronavirus 2 in  
1688 Patients With Coronavirus Disease 2019. *Clin Infect Dis* 71, 713-720.

1689 Stukalov, A., Girault, V., Grass, V., Karayel, O., Bergant, V., Urban, C., Haas, D.A., Huang, Y.,  
1690 Oubraham, L., Wang, A., *et al.* (2021). Multilevel proteomics reveals host perturbations by  
1691 SARS-CoV-2 and SARS-CoV. *bioRxiv*, 2020.2006.2017.156455.

1692 Teodori, L., Sestili, P., Madiati, V., Coppari, S., Fraternali, D., Rocchi, M.B.L., Ramakrishna, S.,  
1693 and Albertini, M.C. (2020). MicroRNAs Bioinformatics Analyses Identifying HDAC Pathway as  
1694 a Putative Target for Existing Anti-COVID-19 Therapeutics. *Front Pharmacol* 11, 582003.

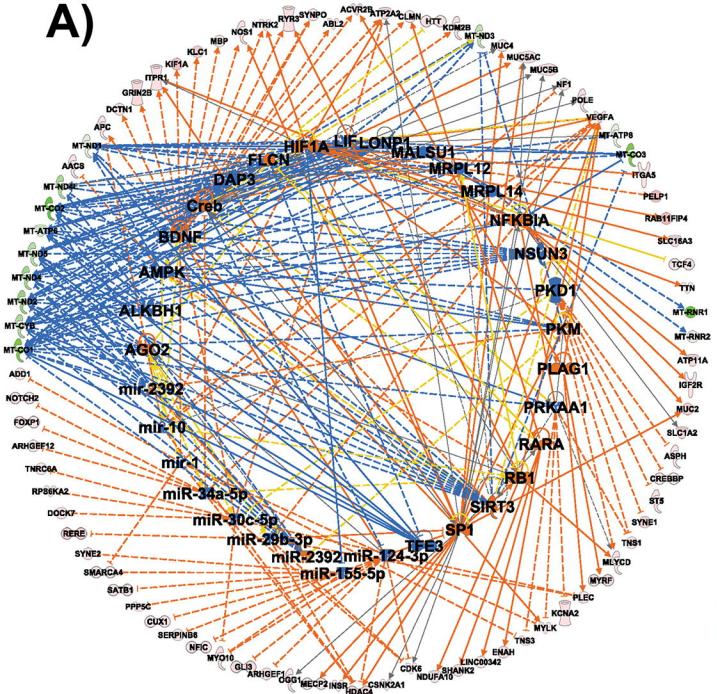
1695 Widiasta, A., Sribudiani, Y., Nugrahapraja, H., Hilmento, D., Sekarwana, N., and Rachmadi, D.  
1696 (2020). Potential role of ACE2-related microRNAs in COVID-19-associated nephropathy.  
1697 *Noncoding RNA Res* 5, 153-166.

1698 Zhang, S., Amahong, K., Sun, X., Lian, X., Liu, J., Sun, H., Lou, Y., Zhu, F., and Qiu, Y. (2021).  
1699 The miRNA: a small but powerful RNA for COVID-19. *Brief Bioinform* 22, 1137-1149.

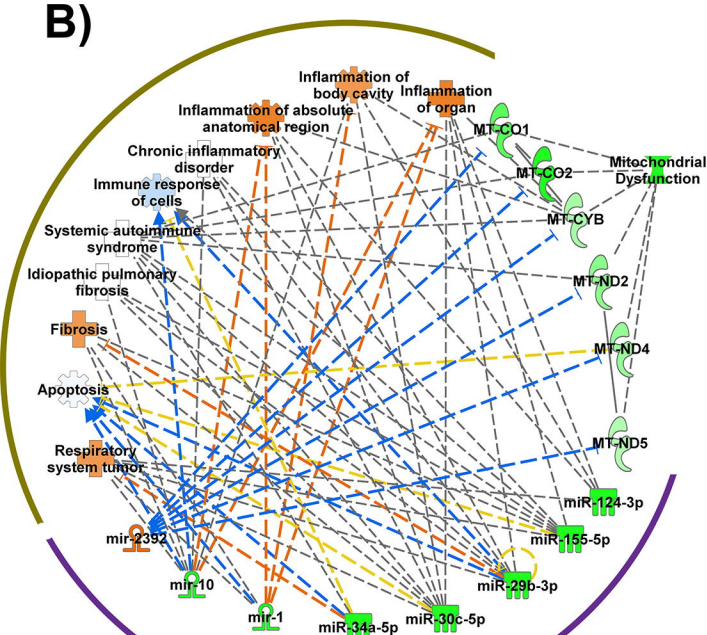
1700



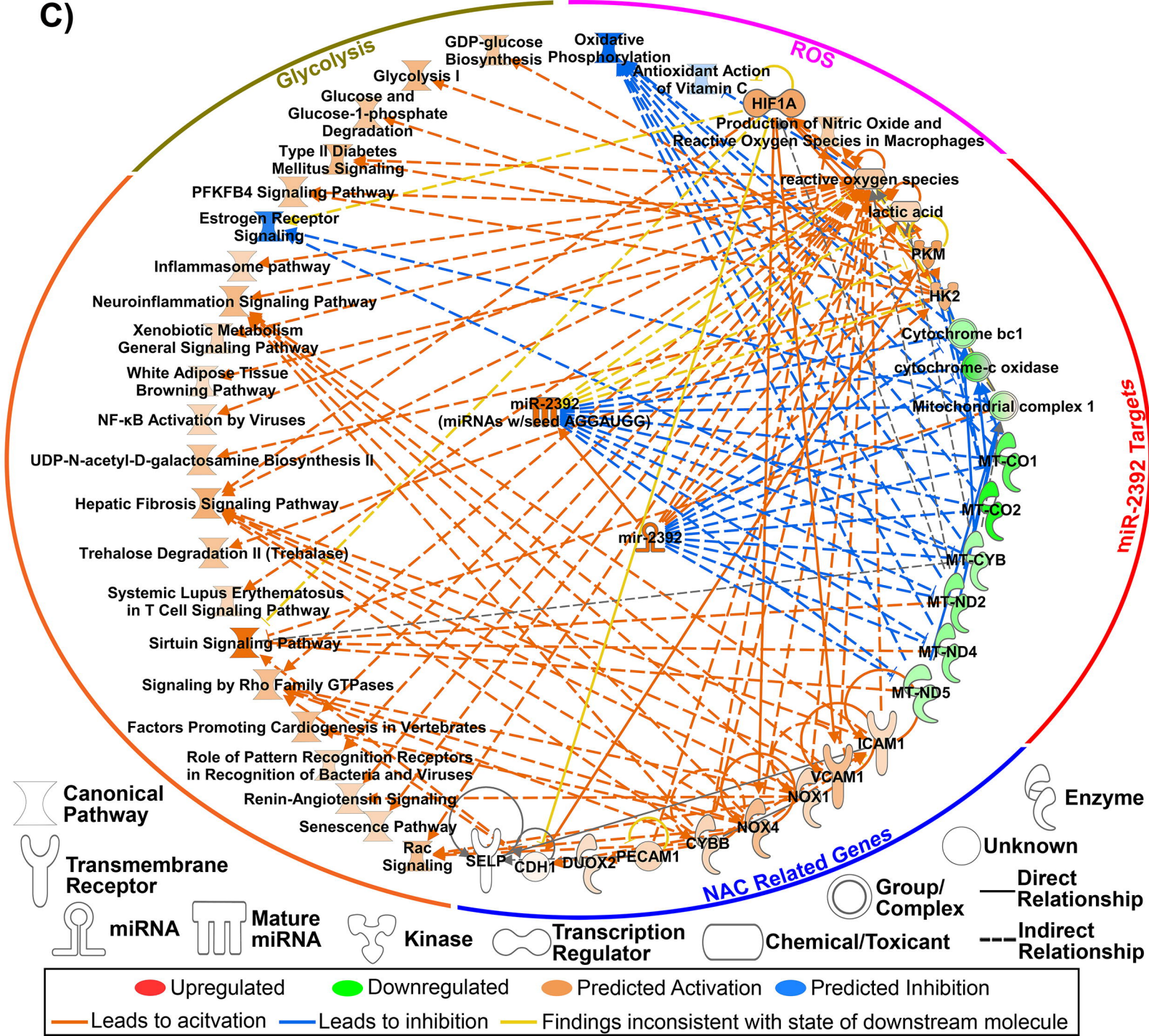
A)



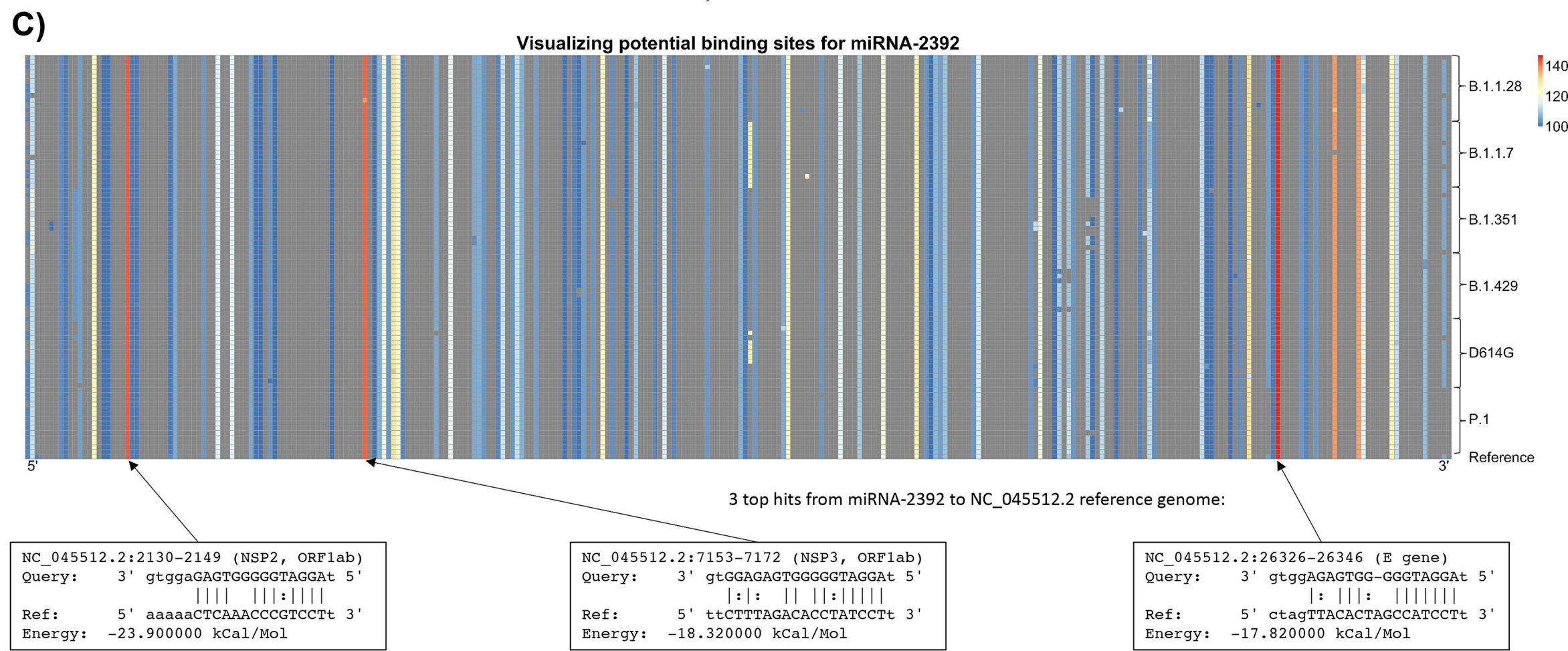
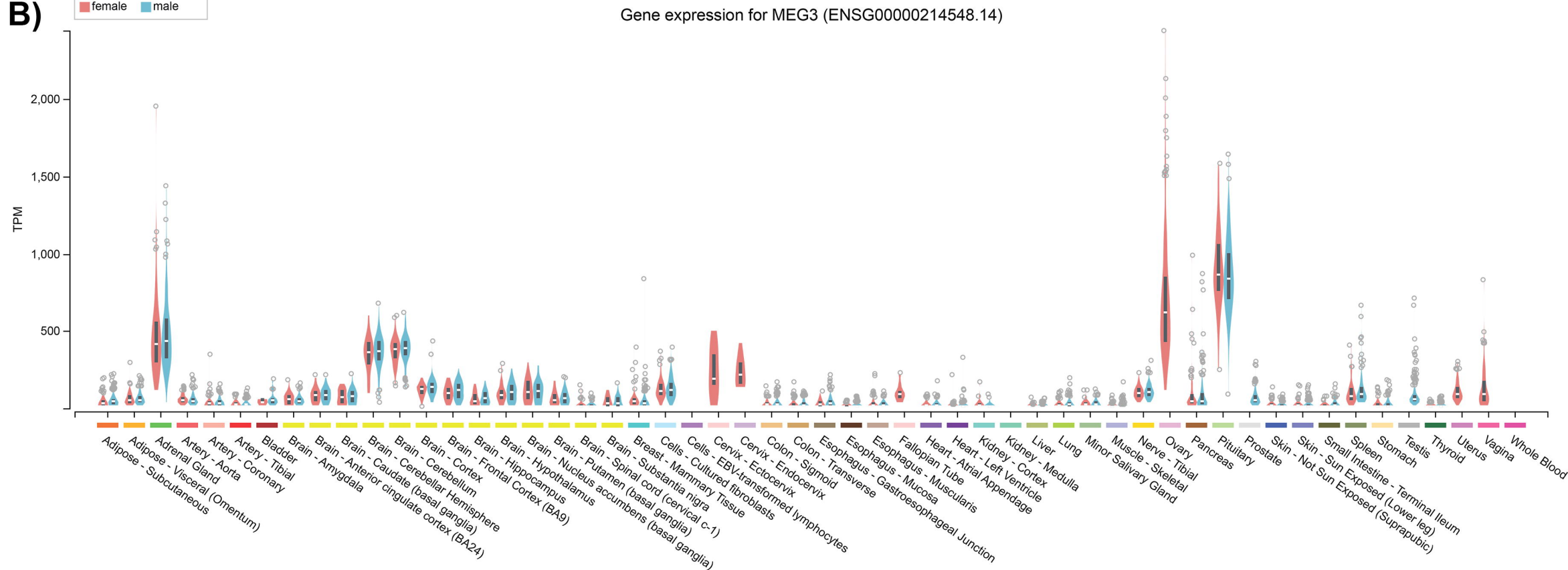
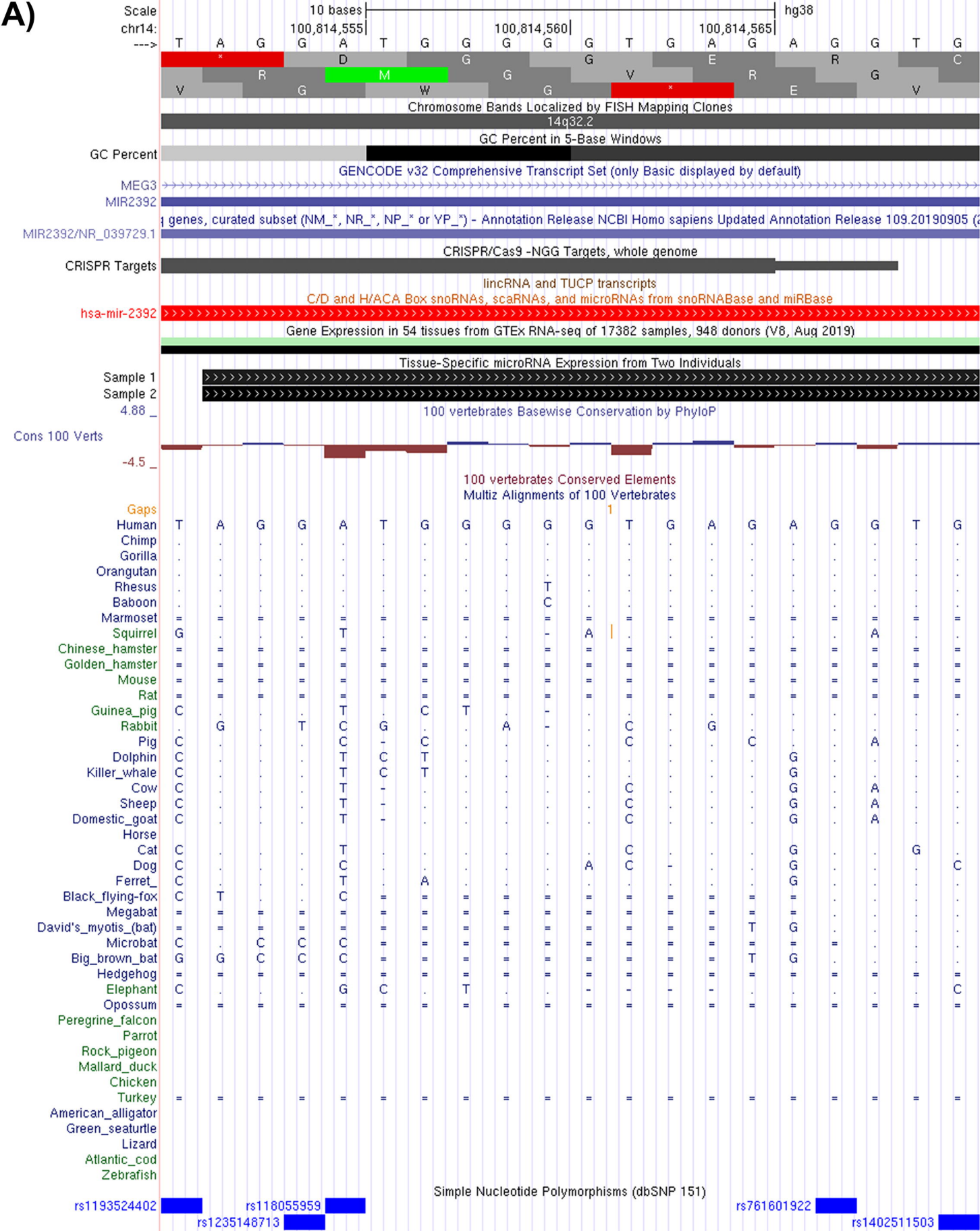
B)



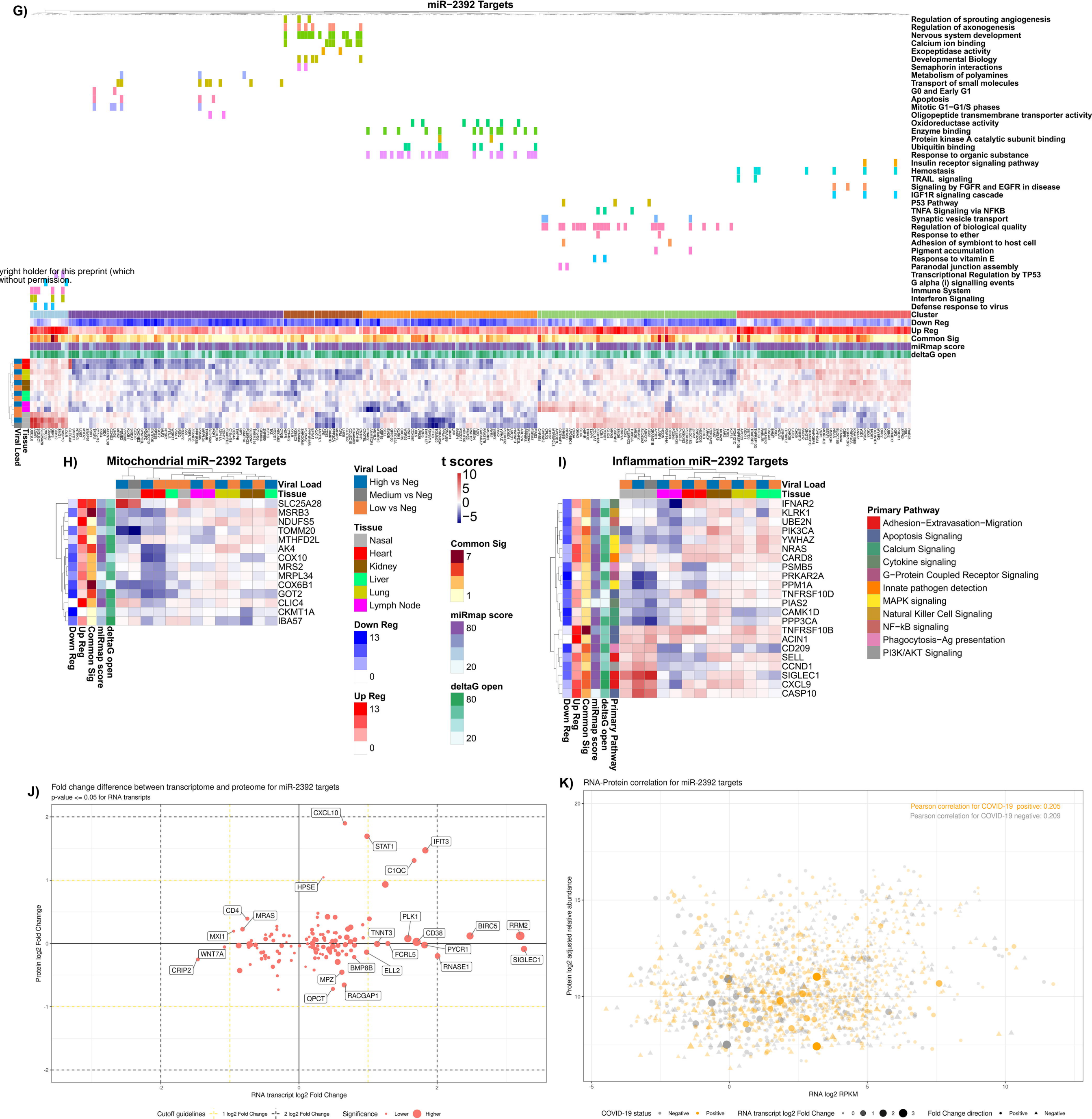
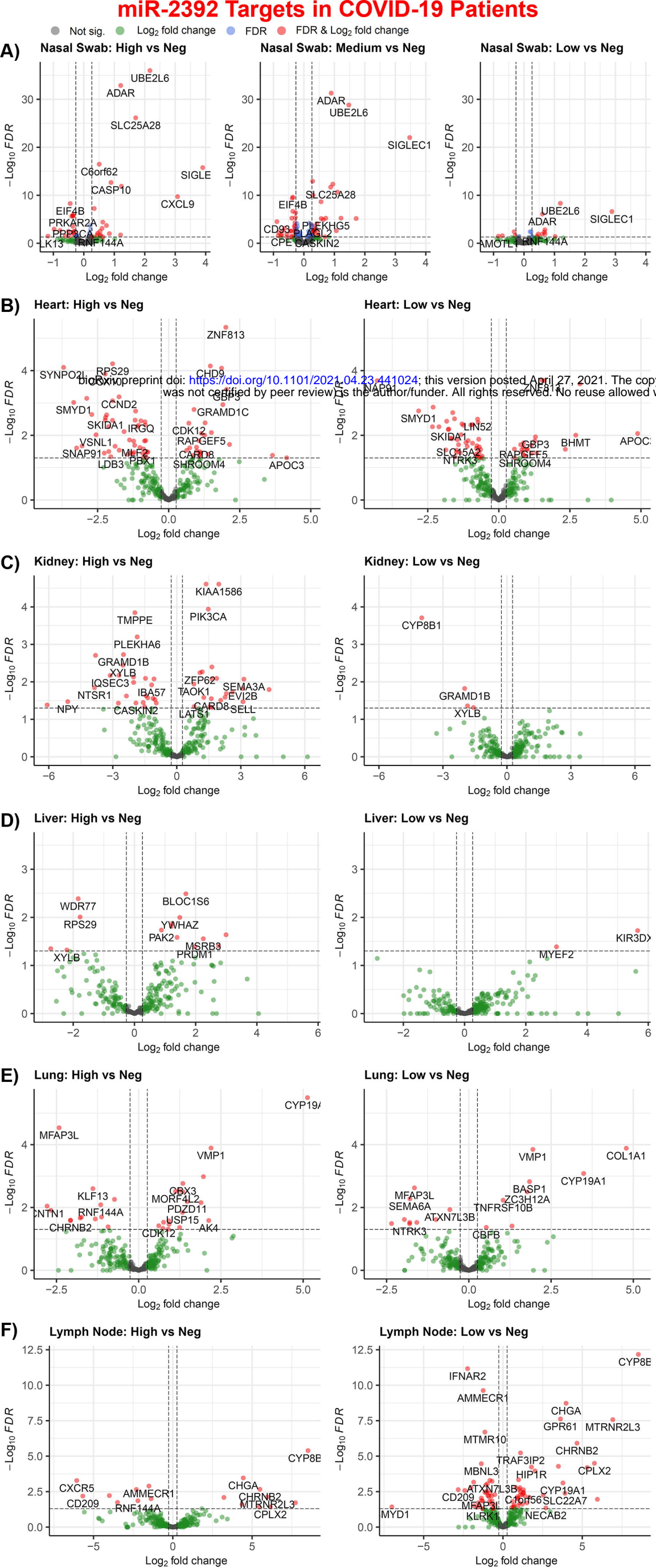
C)



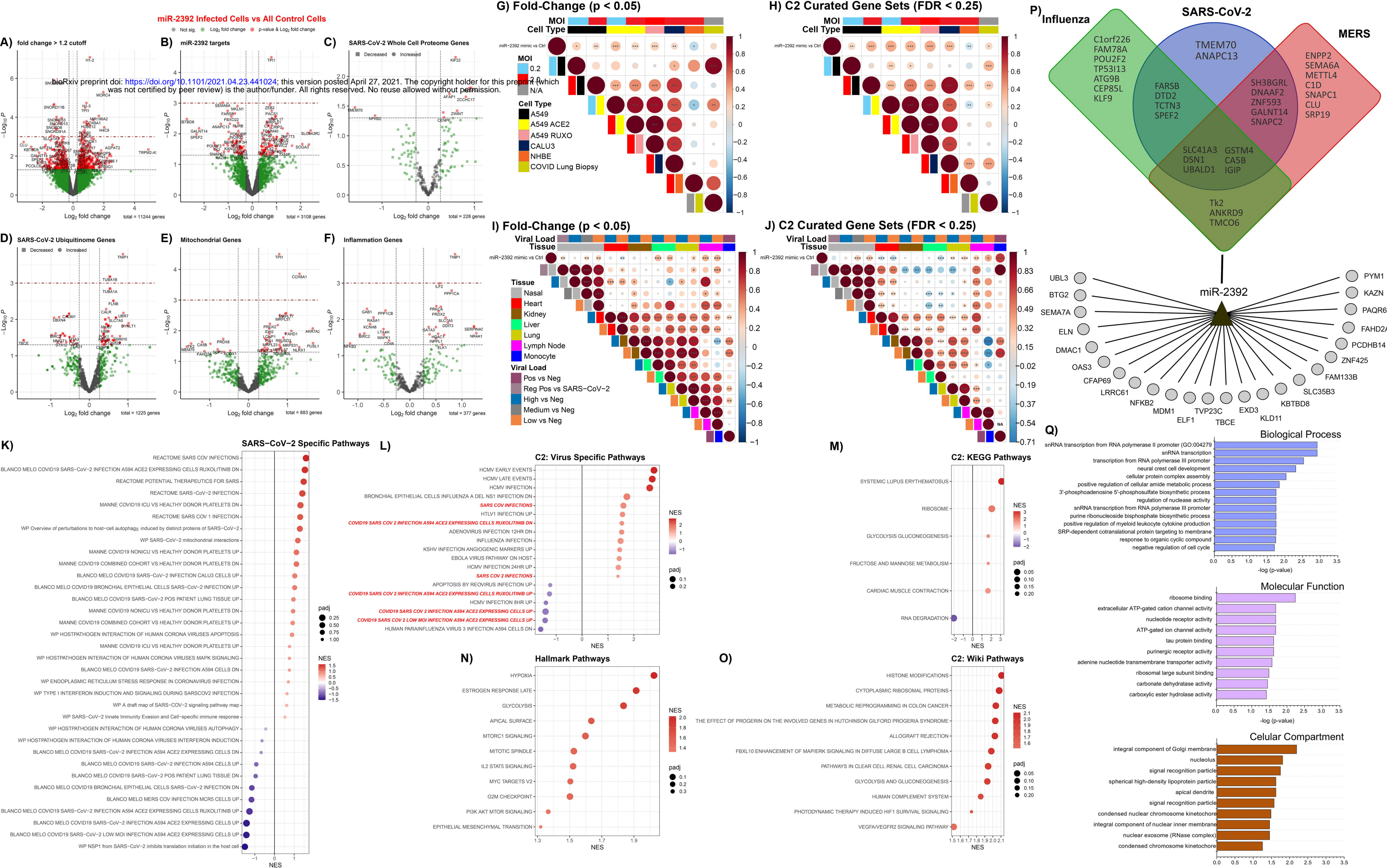




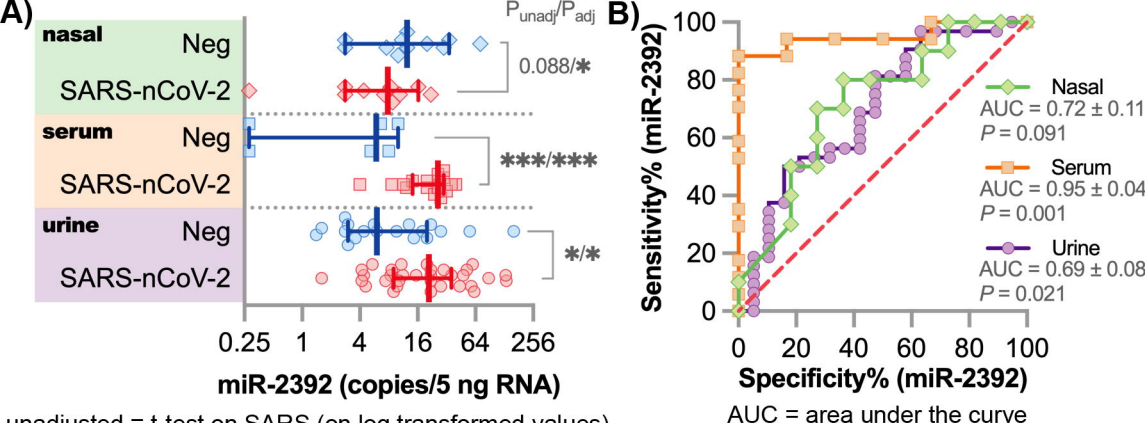




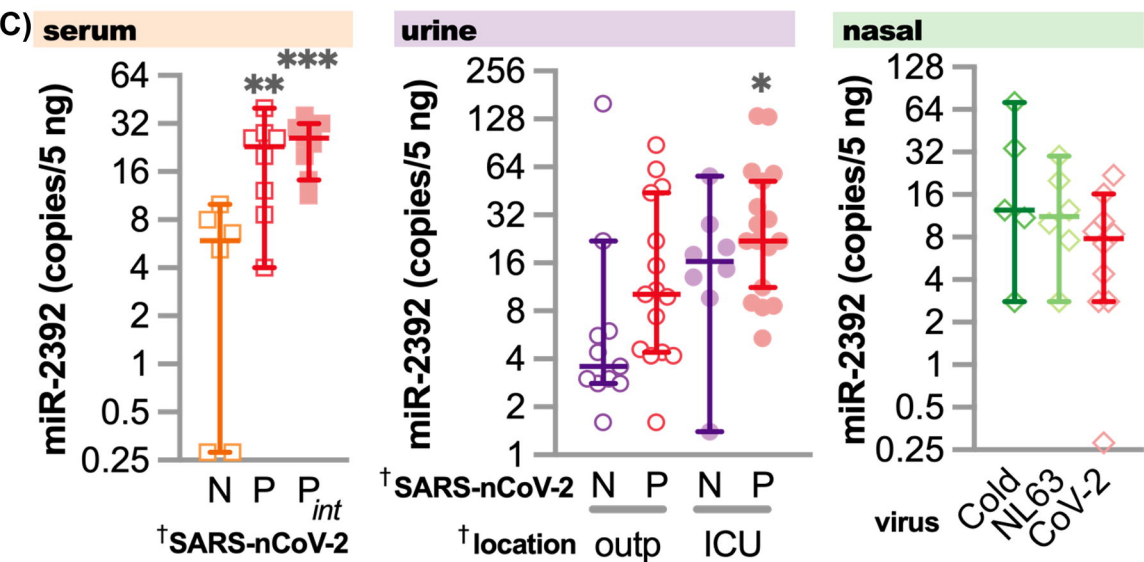








unadjusted = t-test on SARS (on log transformed values)  
 adjusted = mixed model corrected for age and sex (single terms)  
 \*, \*\*, \*\*\* =  $p < 0.05, 0.01, 0.001$



nasal and serum = ANOVA on log values

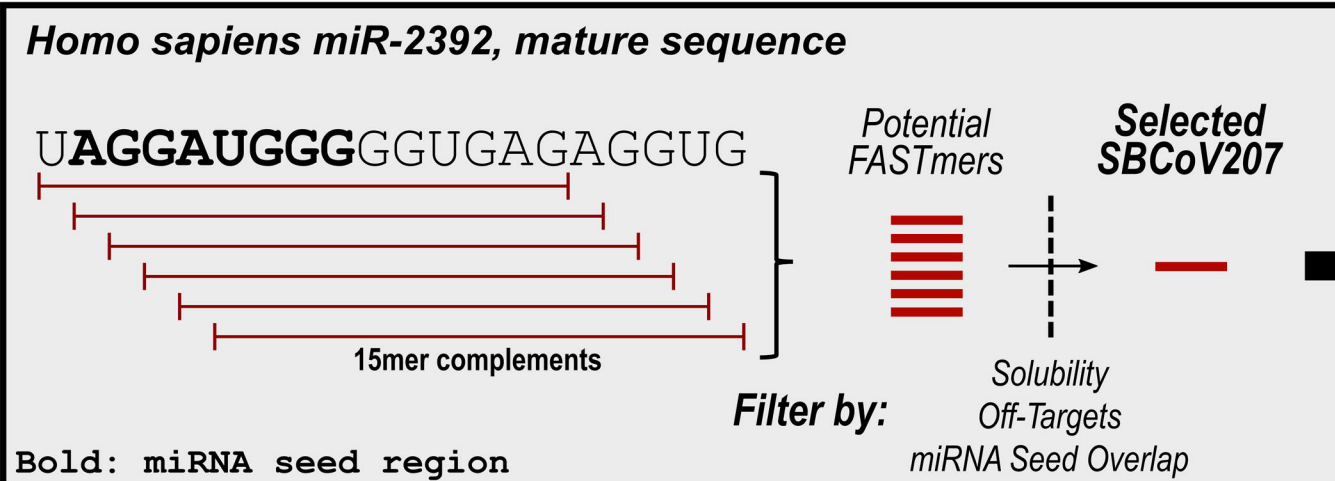
urine = 2-way ANOVA on log values

†, †† =  $p < 0.05, 0.01$  from ANOVA

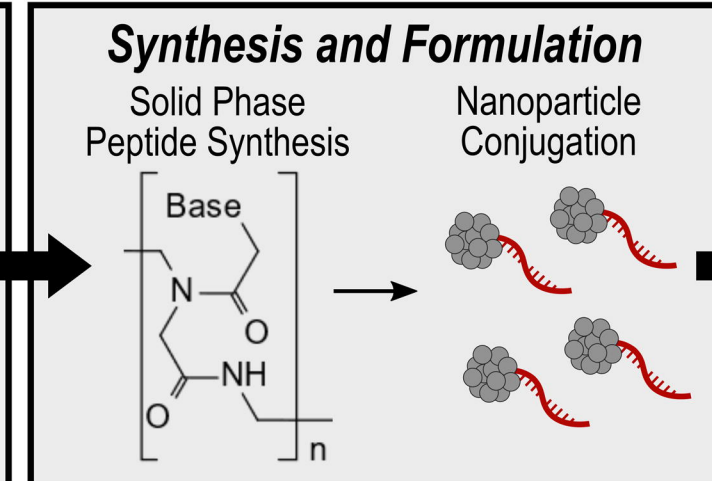
\*, \*\*, \*\*\* =  $p < 0.05, 0.01, 0.001$  from Dunnet's post-test compared to Negative

A)

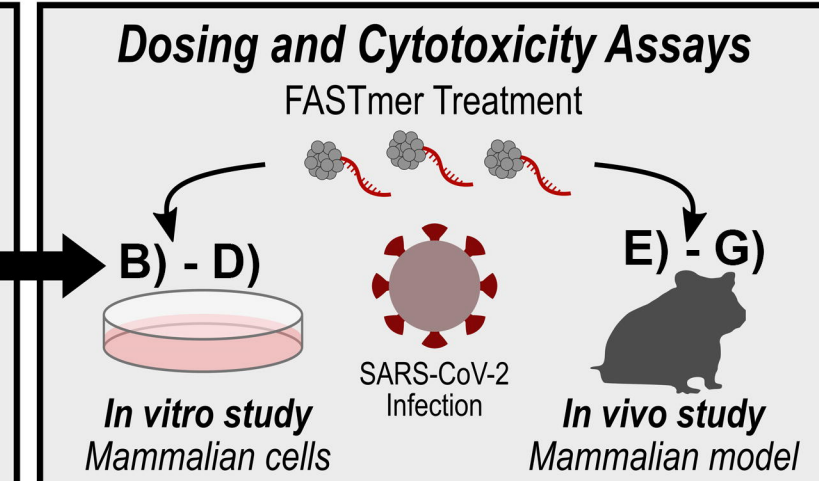
## Design



## Build



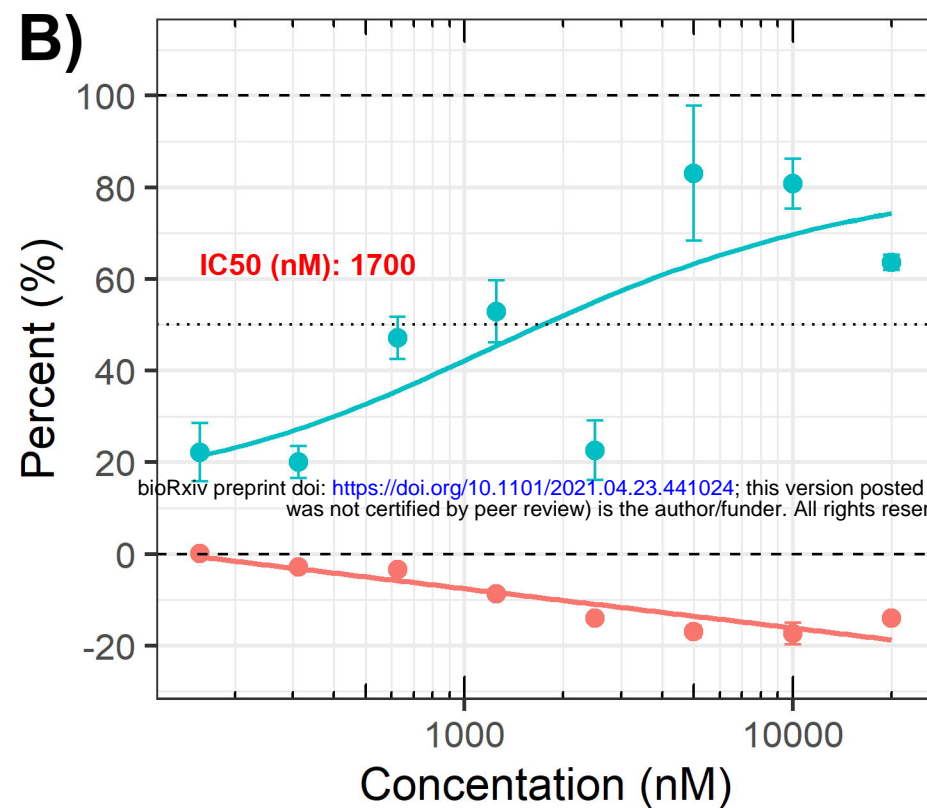
## Test



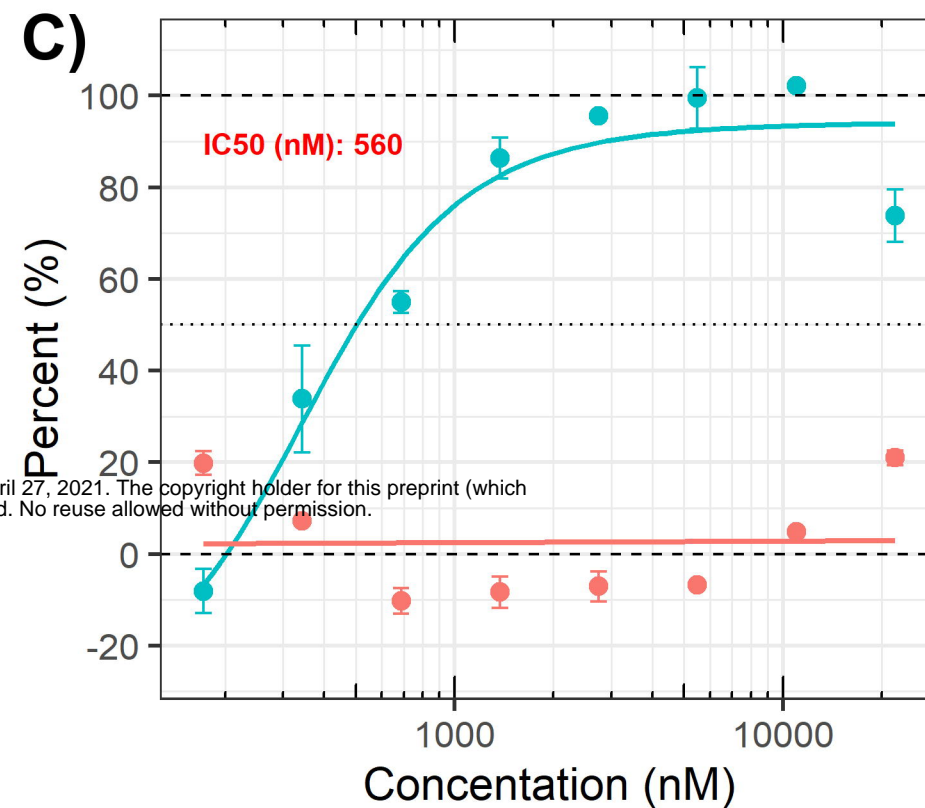
## anti-miR-2392 FASTmer Treatment

● Cytoxicity % ● Inhibition %

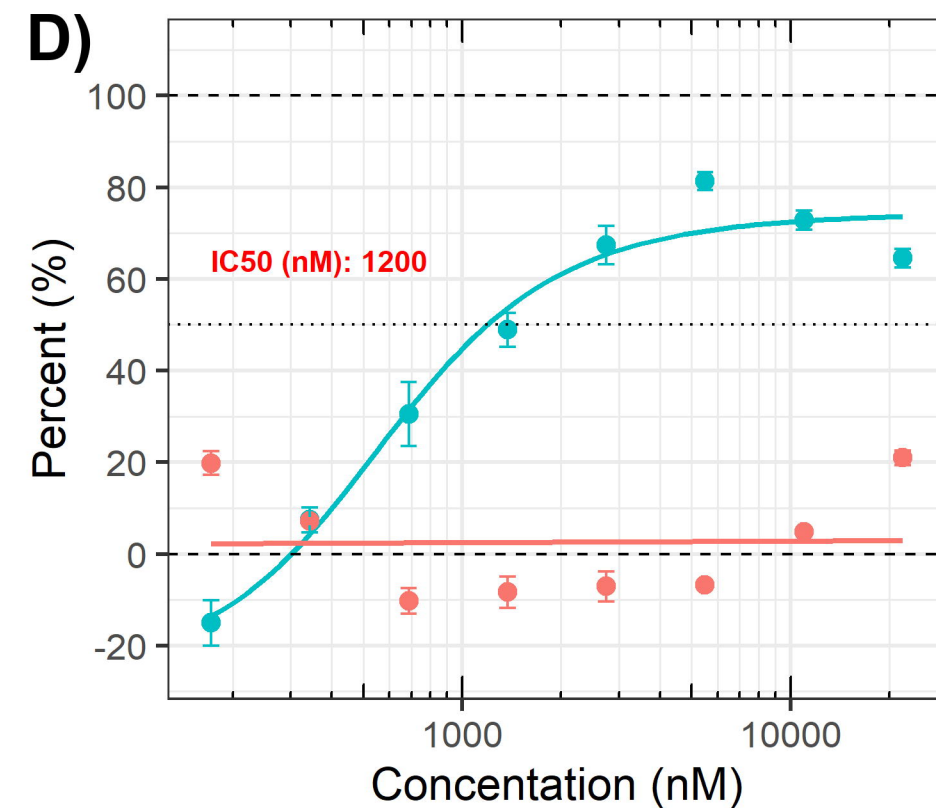
B)



C)



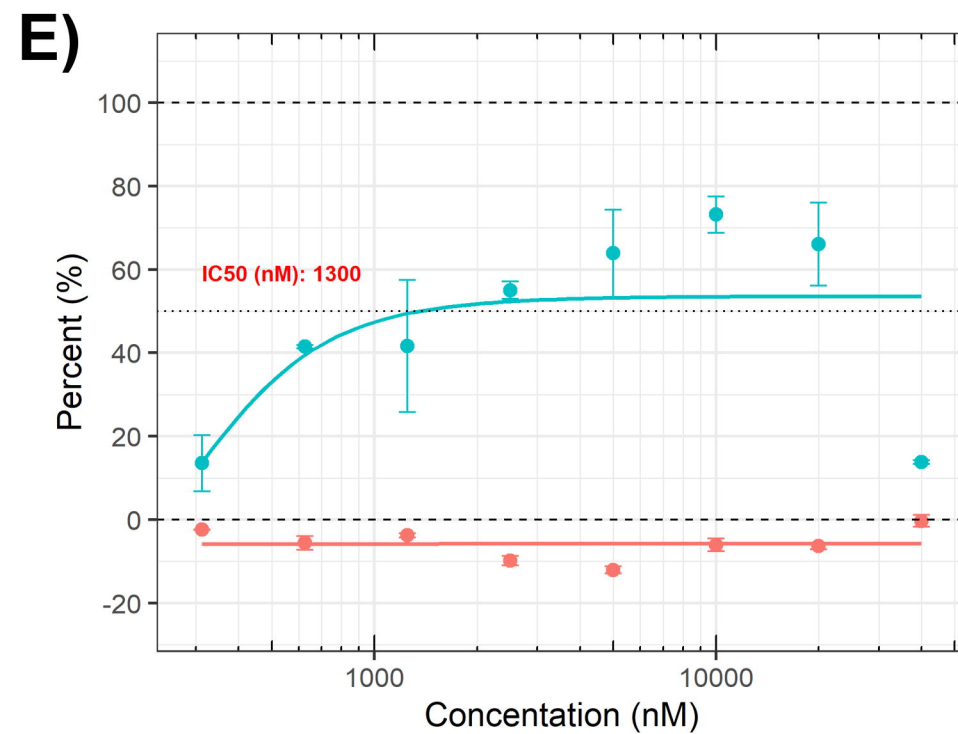
D)



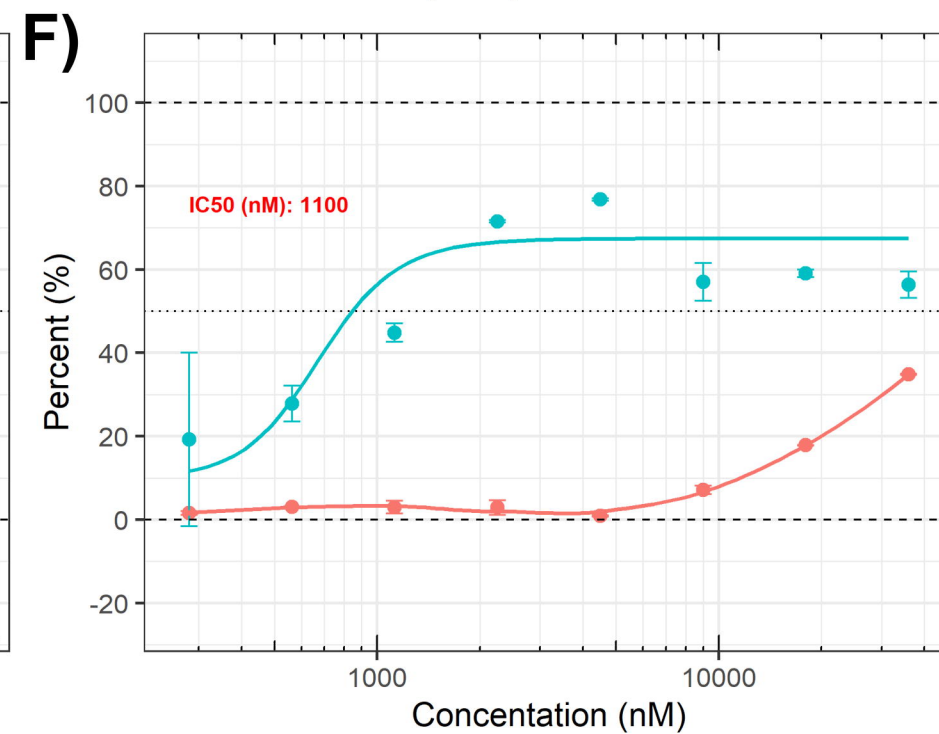
## Nonsense FASTmer Treatment in Human (A549) Cells

● Cytoxicity % ● Inhibition %

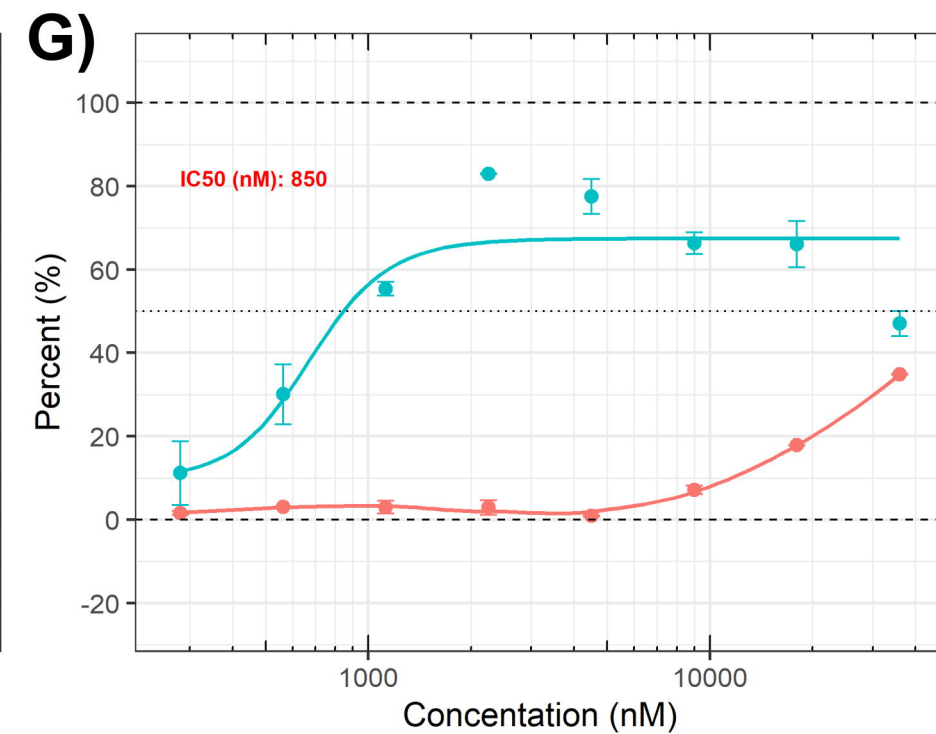
E)



F)

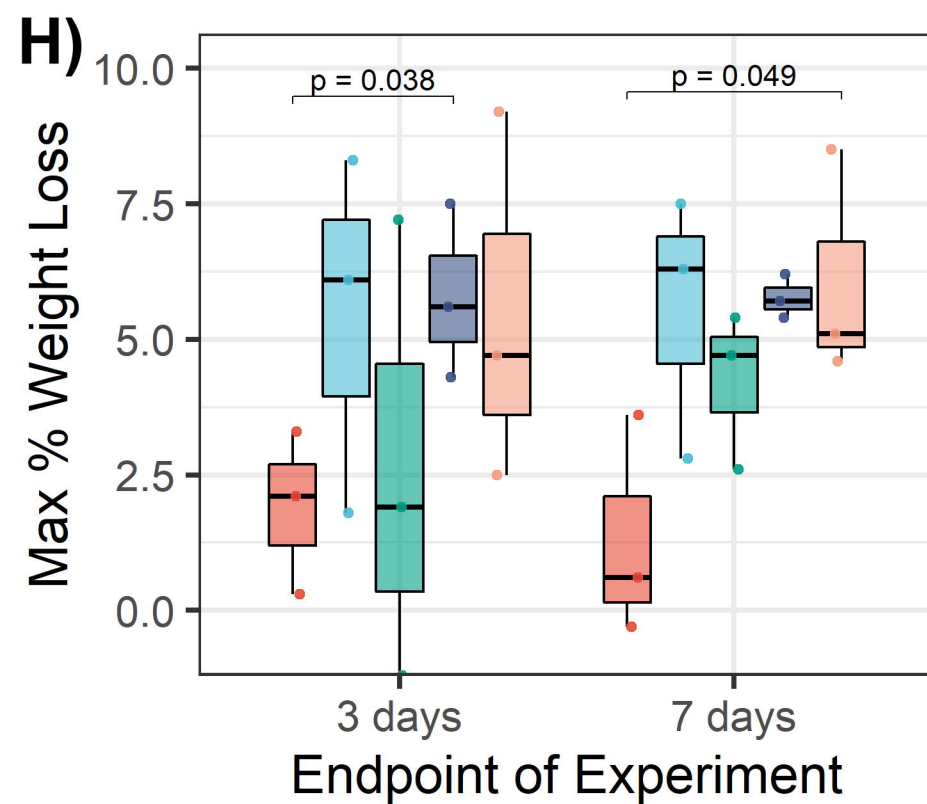


G)

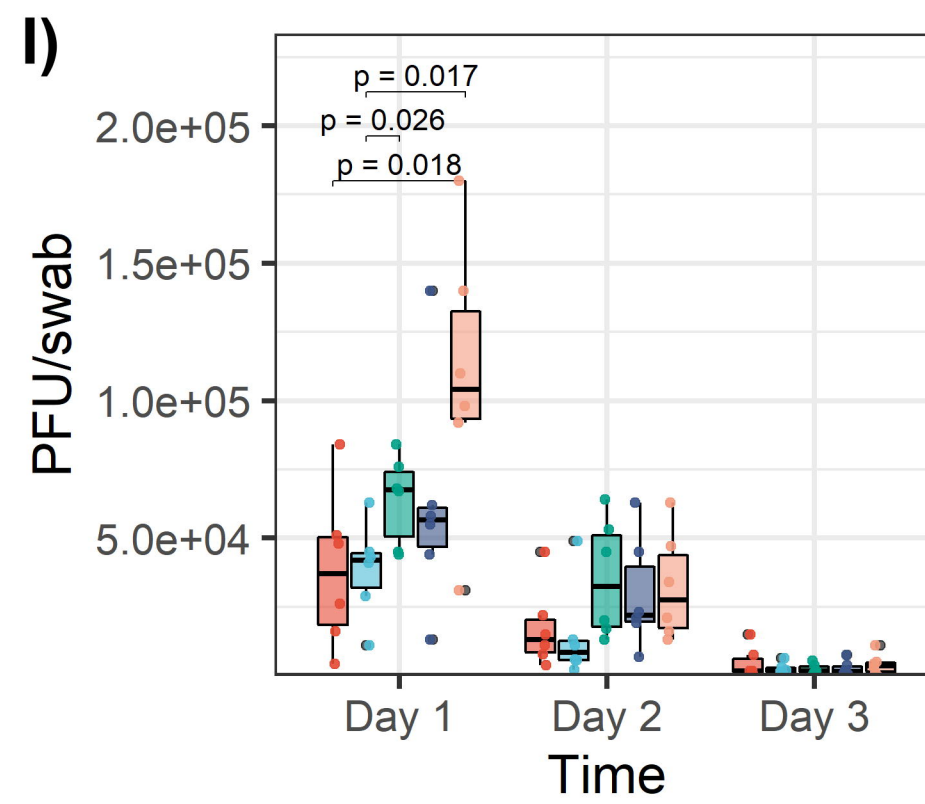


Treatment ■ IN Day -1 ■ IN Days -1, +1 ■ IP Day -1 ■ IP Days -1, +1 ■ PBS IN Days -1, +1

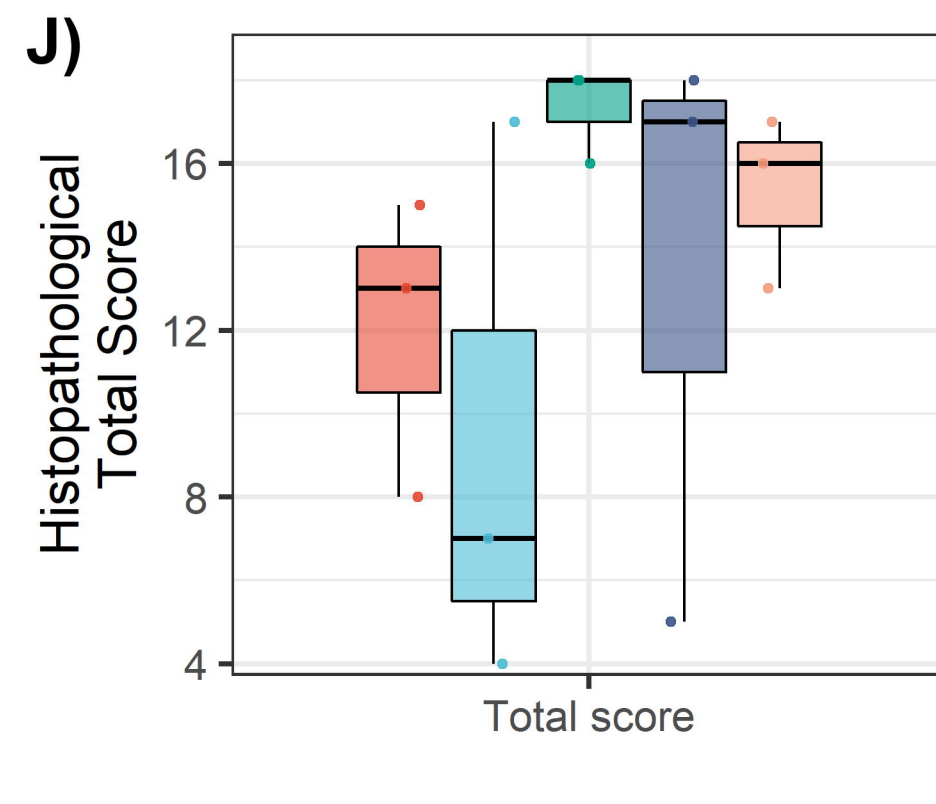
H)



I)



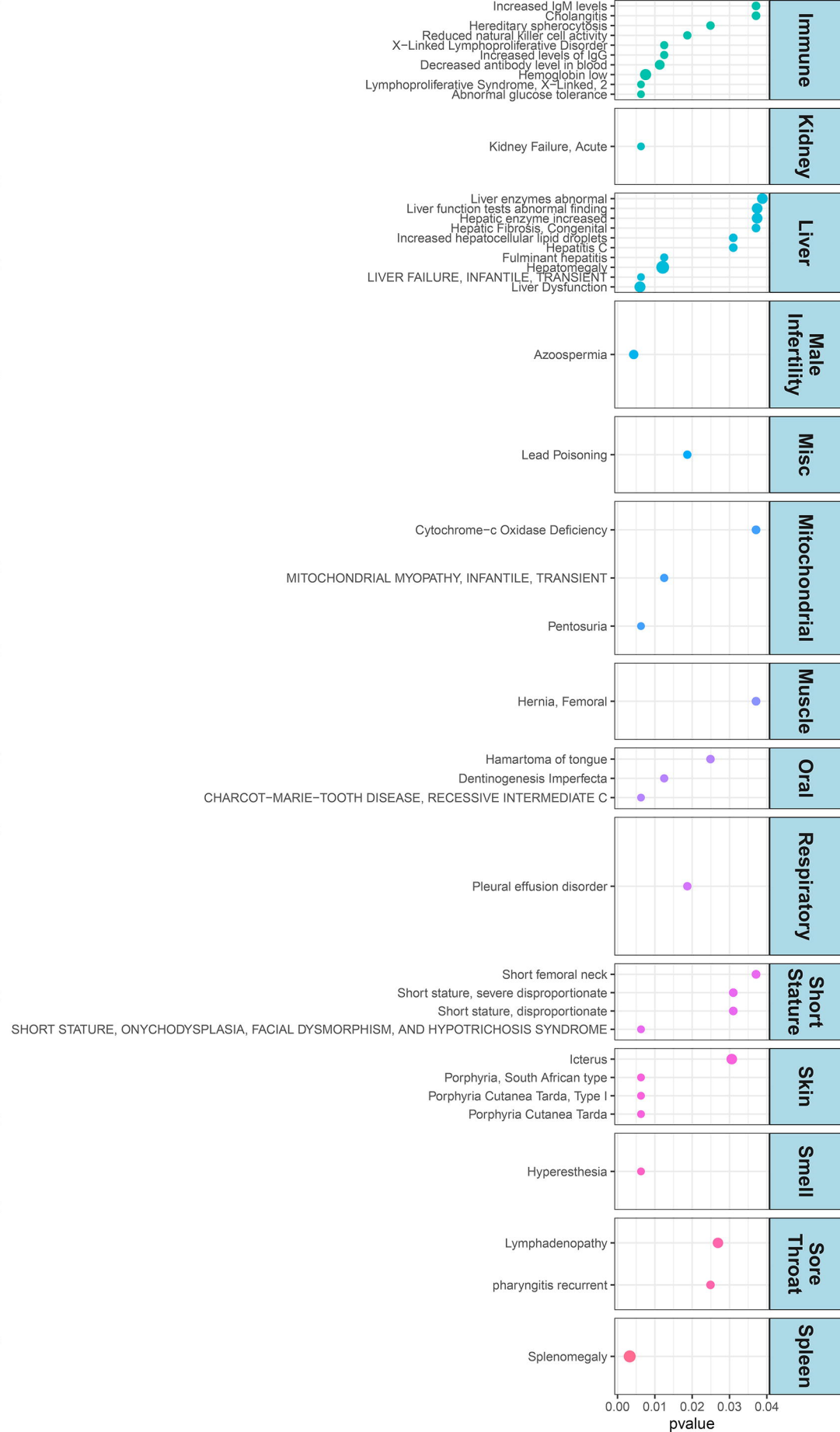
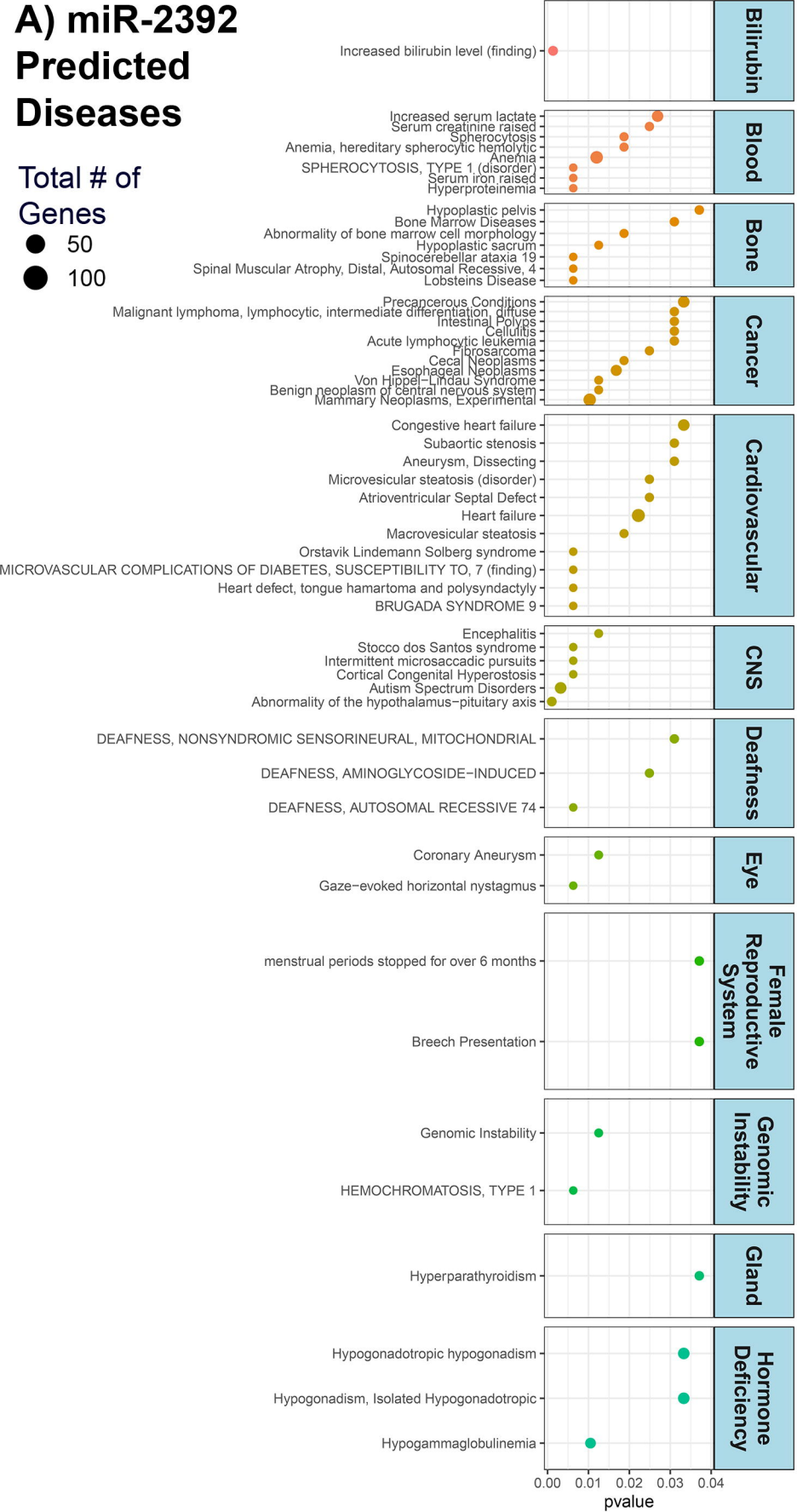
J)



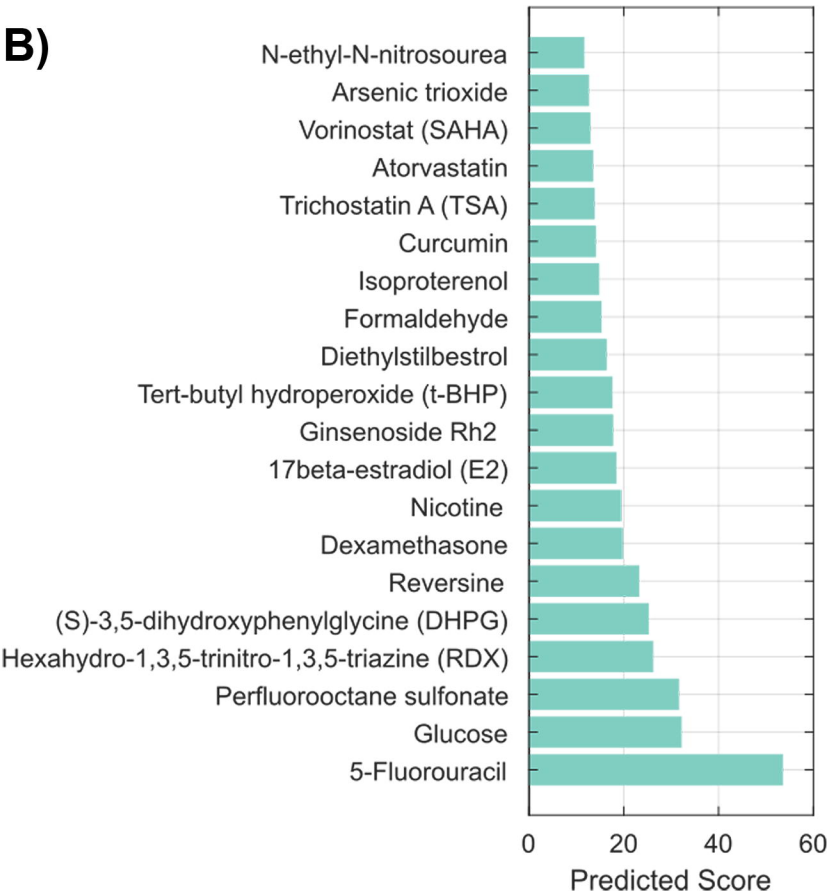


A) miR-2392  
Predicted  
Diseases

Total # of  
Genes  
● 50  
● 100



B)



C)

